Dispersion and abundance of salmon lice (*Lepeophtheirus salmonis*) in a Norwegian fjord system

Master thesis in Physical Oceanography

Ingrid Askeland Johnsen

November 2011

UNIVERSITY OF BERGEN
GEOPHYSICAL INSTITUTE

Acknowledgements

Denne masteroppgåva er skriven i tett samarbeid med Havforskningsinstituttet i Bergen. Eg vil gjerne rette ei stor takk til oseanografigruppa der, for å ha gjeve med tilgang på numerisk data, hydrografiske målingar, samt god hjelp. Ei spesiell takk går til veiledar Lars Asplin, for god motivasjon og hjelp.

Nå og tidligare studentar ved geofysisk institutt vil eg takka for minneverdige pausar.

Sist men ikkje mist: Tusen takk til Gunnar, Vebjørn, øvrig familie og venner for korrekturlesing, støtte og avkobling.

Abstract

Based on numerical results of currents from a high resolution fjord model, dispersion of salmon lice (*Lepeophtheirus salmonis*) in the Hardangerfjord has been modelled. The results show that salmon lice abundance in the fjord have large spatial and temporal variations. Still, enlarged densities of salmon lice occur in certain areas, especially along shores, in bays and in narrows. If there exist a critical dose of salmon lice copepodid density necessary to infect the salmonid fish, the model results of salmon lice dispersion can be used to design a management strategy for salmon aquaculture.

Contents

CHAPTER 1

Introduction

Lepeophtheirus salmonis is a marine parasite feeding on skin and mucus from *Salmo salar* (salmon) and *Salmo trutta* (sea trout) [Heuch and Karlsen, 1997]. It is the dominating sea lice in Northern Europe [Bengtsen, 2011], and its infection on fish may cause osmotic problems leading to reduced growth and increased mortality [Stien et al., 2005]. The purpose of this thesis have been to examine the dispersion and abundance of *Lepeophtheirus salmonis* in a fjord system using numerical models. *Lepeophtheirus salmonis* will from now on be referred to as salmon lice.

Farming of salmon in Nowegian fjords has been an industry adventure since the late 1960's. The production have generally been increasing and during 2010 the production was over 900 000 ton salmon [Directory of Fisheries, 2011]. There have been some draw backs with diseases, but most have been solved under way. Since the mid 1070s the existence of salmon lice in fish farms have been a problem in Norwegian fjords. It is still an unsolved issue. In addition to being a fish health problem, it leads to great financial expenses. In Norway alone it is estimated to cost the industry between 1 and

1.5 billion Norwegian Kroner [Directory of Fisheries, 2011].

The number of farmed fish is now 300 times the wild stock in Norwegian fjords. This great number of salmon leads to a potentially large number of lice produced in the fjords [Heuch and Mo, 2001]. The salmon lice have increased reproduction and probability of survival with higher temperature [Johnson and Albright, 1991b] and [Boxaspen and Næss, 2000]. This normally leads to increasing amount of salmon lice in the fjords during spring and summer. During the spring the post-smolt from the wild salmon stocks migrates from the rivers to the Atlantic ocean, where it spends most of its life. On its way out of the fjords, it often has to migrate through areas heavily abundant with salmon lice. Due to the post-smolts small size it is especially vulnerable to salmon lice infections. It is likely that salmon lice originating from fish farms infect the wild stock of salmon and sea trout [Otterå et al. [2004]; Heuch and Mo [2001]].

Fish farmers are are obliged to delouse the farms chemically every spring and whenever the number of lice in the farm exceeds a certain limit. A limited capacity of equipment makes it impossible to delouse whole fjords simultaneously, but the authorities tries to synchronize delousing of regions of the fjord in stead. Synchronized fallowing of regions for 1 to 2 months have been introduced by the authorities to reduce the negative effect of pathogen spreading. Knowledge of the abundance of salmon lice in time and space in a fjord area will therefore be important in order to assess this new way of managing fjords. Numerical models of salmon lice dispersion can be an indispensable tool in such a new management regime. Modelling salmon lice dispersion has only been done for approximately 10 years. A few Norwegian groups (especially at the Institute of Marine Research (IMR) and SINTEF) have operational salmon lice models as well as groups in Scotland, Canada and Chile. Altogether the number of scientists involved in such models is low, but the collaboration among them is good. A summary of the state of the art two years ago is given in the Salmon Lice book by Jones and Beamish [2011]. Today the progress of salmon lice modelling has mainly been towards

establishing better forced current models with higher spatial resolution.

The salmon lice has been shown to have a conduct of migrating up when stimulated by light [Heuch et al. [1995]; Bengtsen [2011]]. It has also shown swimming ability when stimulated by infrasonic water oscillations [Heuch and Karlsen, 1997]. However it is believed that it mostly saves its energy. It drifts along the currents, migrating up and down diurnally, and uses its swimming capacity first when a host is detected. The development and ageing of the salmon lice, and hence the time period it is infective is dependent on temperature. When simulating abundance and distribution of salmon lice in a fjord, information of currents and temperature is evidently conclusive. Numerical hydrographic models make a detailed description of currents and temperature, and makes it possible to simulate the growth, abundance and dispersion of salmon lice.

In this thesis the distribution and growth of salmon lice in the Hardangerfjord have been modelled.

The main objective of this thesis has been to examine the following hypotheses:

1. Lice do disperse differently depending on which part of the fjord they originate from.

2. It is possible to define an area that is influenced by lice originating from a given position.

3. The influence area of lice from a given position can be used to estimate the size of the regions of synchronized delousing and fallowing.

The Hardangerfjord was chosen as the area of investigation due to a wide dataset provided by the Institute of Marine Research (IMR). A hydrographic model for the Hardangerfjord has been used to obtain detailed data of the fjord currents for the spring of 2007, and has made it possible to simulate the dispersion of salmon lice in the fjord. Observations of currents, temperature and salinity have been used to describe the fjord circulation and in purpose of model validation.

1.1 The Hardangerfjord

The Hardangerfjord is situated at the Western coast of Norway (Figure 1.1). With the fjord mouth placed approximately at 59.5°N, 5°E and the head at 60.5°N, 7°E. The fjord is over 150 km long from the fjord mouth to Eidfjord (Figure 1.1), making it the second longest fjord in Norway. The fjord system consists of several branches, with many smaller side fjords all with different names. Even the main fjord itself has different names. For simplicity the whole fjord system from mouth to head will be referred to as the Hardangerfjord in this thesis. When referring to smaller areas of the fjord, the names in Figure 1.1 and sections shown in Figure 1.3 defined by the IMR, will be used.

At the mouth the fjord is approximately 4 km wide. Further into the fjord, the width at some places is nearly doubled. The bottom has several sills. At the mouth of the fjord the depth is about 150 m. Moving inward, the fjord is deeper, but seldom exceeds 400 m. North of Halsnøy (Figure 1.1) there is a second sill at 150 m. Inside this second sill the depth increases, reaching maximum at almost 850 m outside Jondal (Figure 1.1) [Ervik et al., 2008].

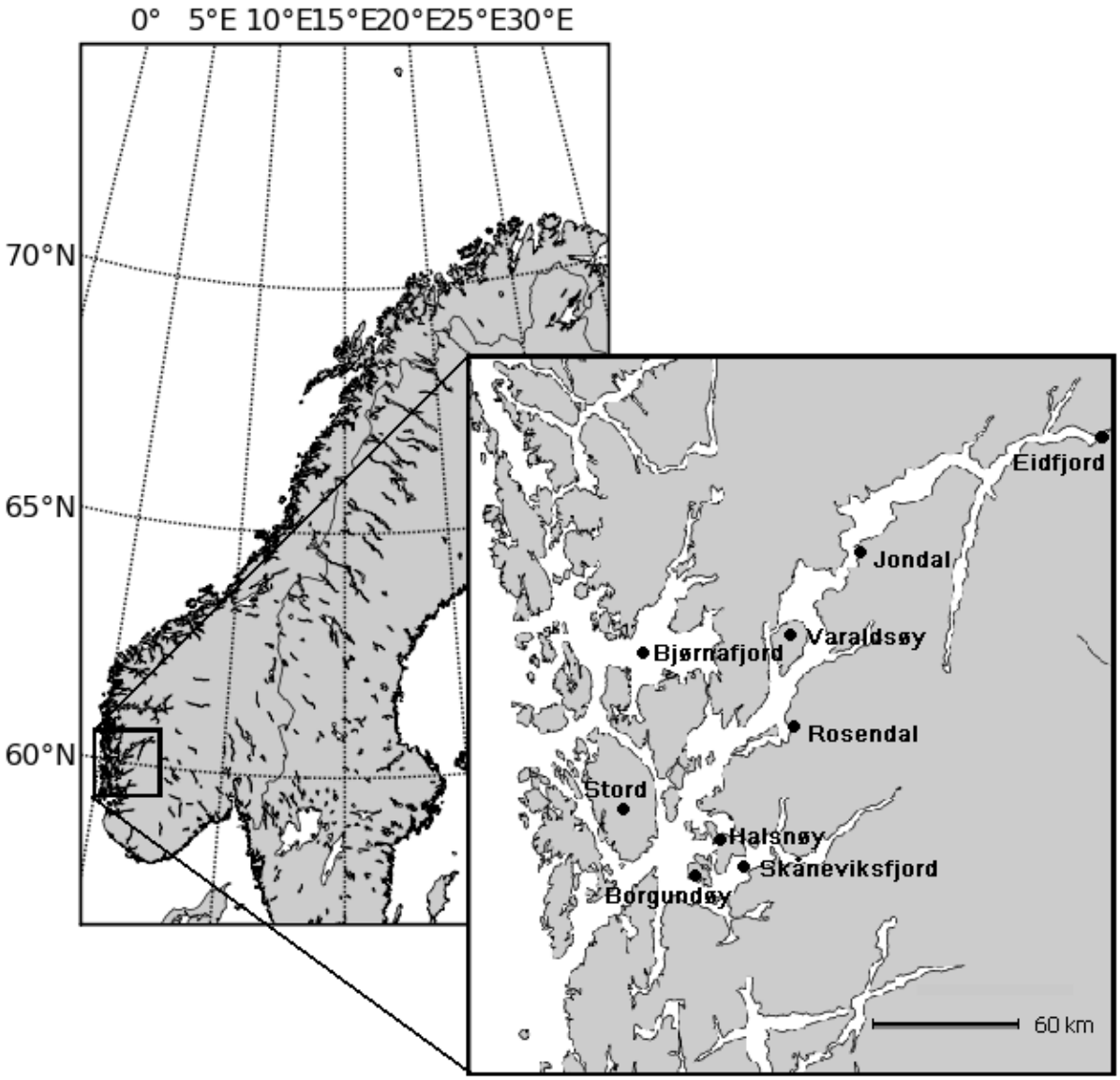

Figure 1.1: *The Hardangerfjord.*

The inner part of the fjord is surrounded by steep mountain slopes. Southwest of Varaldsøy the steepness of the mountain slopes decreases, leading to a more open landscape outside Rosendal (Figure 1.1). The Hardangerfjord forms a peninsula at which the third largest glacier in Norway is located, Folgefonna. Air masses being cooled over the cold glacier may generate downslope winds that are channelled along the fjord by the steep topography.

1.2 Data

Hydrographic measurements and model results used in this study are provided by the IMR. Hydrographical measurements have been carried out for several decades, but the year 2007 is examined in this thesis, as a simulation of the fjord hydrography was available for this year.

The fjord model the Regional Ocean Model System (ROMS) was set up for the area showed in Figure 1.2 and simulated the fjord hydrography of the spring 2007. A description of the model will be given in Chapter 2.3

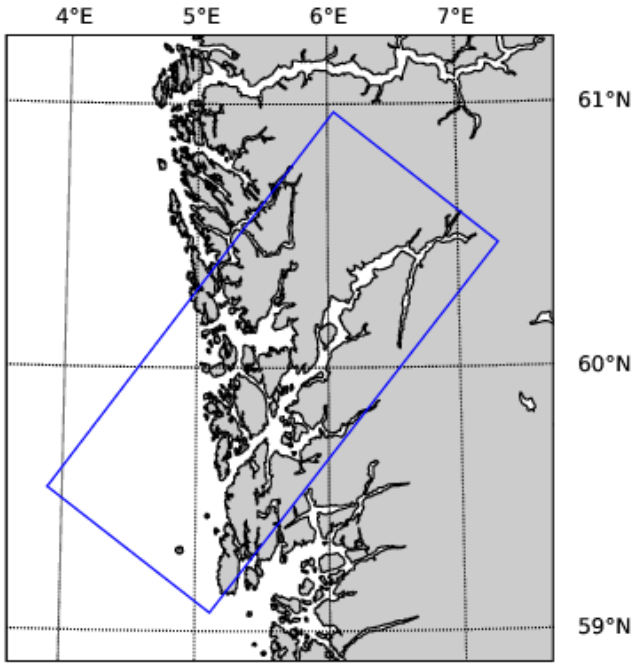

Figure 1.2: *The model domain of the ROMS model for the Hardangerfjord (blue rectangle).*

Hydrographic measurements were carried out several times during the spring 2007. The positions of the measurements are given in Figure 1.3. Temperature and salinity measurements were obtained twice, and currents measured giving time series that covers most of the examined period of this thesis. The positions and time of the measurements used in this study are given in Figure 1.3 and Table 1.1 respectively.

Conductivity, Temperature and Depth (CTD) were measured at stations in the H-sections shown in Figure 1.3. The instrument used is the Saiv SD 204. It measures sea water conductivity, temperature and depth (pressure) and calculates salinity and water density. The sample rate was set to

1 second and the lowering speed was less than 0.5 m/s. Post processing has been made, giving a vertical resolution of 0.1 m the top 5 meters, and 1 m at greater depth.

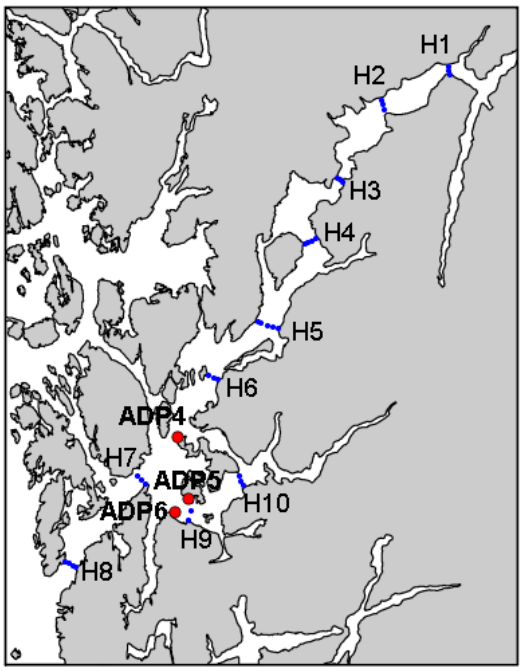

Figure 1.3: *CTD and ADP stations*

Table 1.1: *Data used in this thesis. Retrieved by the IMR.*

Measurements and numerical models	**Stations**	**Period**
Fjord model (ROMS)	Area marked in Figure 1.2	15.04.2007-31.06.2007
CTD	section H1 - H10	07.05.2007-08.05.2007
	section H1 - H8	08.06.2007-09.06.2007
	section H2	25.03.2008
	section H2	17.06.2008
ADP	ADP4, ADP5, ADP6	06.05.2007-28.08.2007
Salmon lice growth and advection model (Ladim)	U1-U12	02.05.2007-09.06.2007

Accoustic Doppler Profiler (ADP) was deployed at the ADP stations shown in Figure 1.3 for spring and summer 2007 (dates are given in Table 1.1). The instrument used was a Nortek Aquadopp vertical profiler, measuring the horizontal and vertical velocities from the instrument and upwards with a range of 40 m. Pressure and temperature are also measured at the instrument depth. Internal sensors give the tilt and compass direction of the instrument (Nortek AS [2006]). The velocities are later decomposed into components along and across the fjord axis.

CHAPTER 2

Theory & methods

2.1 Fjord hydrography

The salinity and temperature distribution is of importance for salmon lice growth and behaviour, as well as the currents, that mainly determine their advection. Thus we need detailed information on fjord hydrography in order to simulate the dispersion of salmon lice.

The factors controlling the currents and temperature in a fjord are many. Heat from the atmosphere, fresh water from precipitation and run-off from land affects the temperature and density stratification in the fjord. Together with wind, tides and the water mass variability outside the fjord they are the main driving forces affecting the water in a fjord. Steering factors as topography and the Coriolis effect are also of importance controlling the hydrography of a fjord.

Heat is being transferred to the sea through radiation from the sun and the atmosphere, and heat conductivity and latent heat at the sea surface. The heat balance describing sources and sinks of heat for the ocean is given

in Equation 2.1 [Wallace and Hobbs, 2006]. Here we look at the surface as an infinitely thin surface, with no heat capacity.

$$FS_{in} + FS_{ref} + FL_{in} + FL_{out} = HS + HL + C \tag{2.1}$$

The variables are described in Table 2.1.

Table 2.1: *Description of the variables of Equation 2.1*

FS_{in}	Solar radiation
FS_{ref}	Reflection of solar radiation
FL_{in}	Incoming long wave radiation
FL_{out}	Emitted long wave radiation
HS	Sensitive heat
HL	Latent heat
C	Conductivity downwards of heat

The fluxes are said to be positive when they are directed downwards and are heating the water. The solar radiation (FS_{in}) and incoming long wave radiation (FL_{in}) are always positive. The incoming long wave radiation is mainly emitted from clouds and the atmosphere. The reflection of solar radiation (FS_{ref}) and emitted long wave radiation (FL_{out}) can only be negative.

The sensible heat flux (HS) is positive when the atmosphere is warmer than the ocean, and negative when the situation is opposite. The magnitude of the the sensible heat flux is dependent on the temperature difference. Latent heat (HL) is mostly negative for the ocean. When the atmosphere gains moisture from the ocean, the ocean loses energy and hence heat. The latent heat flux is therefore dependent on the water content of the atmosphere. Warm dry wind over the ocean results in a large negative latent heat flux. The heat conducted into the water (C) is the actual heat gain or loss of the fjord [Wallace and Hobbs, 2006].

According to Equation 2.1 the radiative terms must be equal to the sum of sensible heat, the latent heat and the conductivity of heat downwards into

the ocean. The atmosphere has lower heat capacity than water, and hence fluctuates more rapidly. Thus the heat flux fluctuates both diurnally and seasonally.

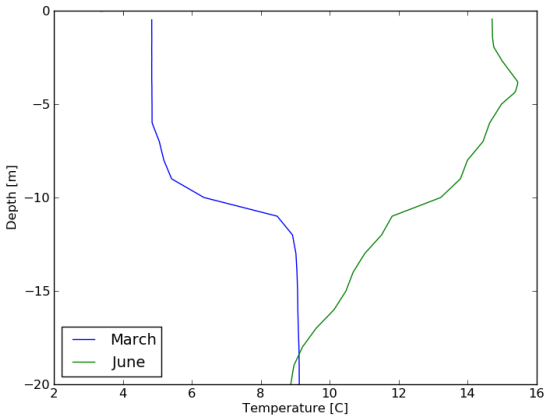

Figure 2.1: *Temperature [°C] at H2.2 March and June 2008 (winter and summer situation).*

Following the seasonal temperature in the atmosphere, the heat flux is normally at its largest during the spring. This results in a maximum temperature at the surface in the summer, normally July - August for the Hardangerfjord according to Svendsen et al. [1972-73]. During wintertime the ocean is warmer than the atmosphere. The heat is transferred from the water to the atmosphere and the heat flux is negative. When looking at a high latitude fjord system, such as the Hardangerfjord, the heat flux is negative most parts of the year. Since atmospheric heating cause water close to the surface to be warmed in a greater extent than deeper down, a positive heat flux is generally stabilizing the water column. In the same way a negative heat flux during wintertime might lead to unstable conditions, increasing downward mixing. The heat flux from the atmosphere can be observed down to 100-150 m depth in the Hardangerfjord [Svendsen et al., 1972-73], with a time delay increasing with depth. At 150 m depth the temperature reaches its maximum temperature about 6 months after the surface.

Fresh water from precipitation and run-off is supplied to fjords throughout the year. The fresh water added to the fjord makes the water close to the

surface less dense and is the main stabilizing parameter for the stratification and source of buoyancy.

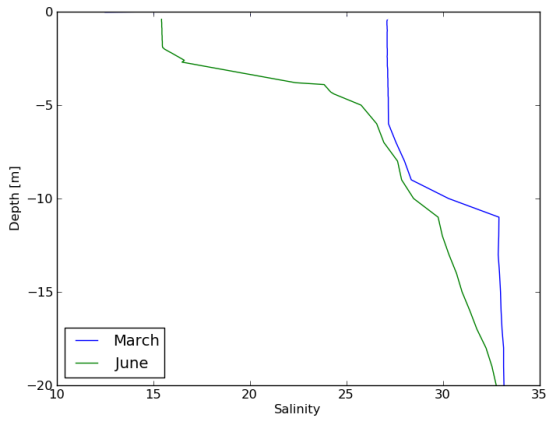

Figure 2.2: *Salinity at H2.2 March and June 2008*

The largest amount of run-off is during the melting season in the spring and early summer. The fresh water supplied to the fjord creates an approximately 5 m thick layer of brackish surface water with low density. A small surface elevation gradient is forcing the brackish water, causing an outgoing current, eventually transporting the supplied freshwater out the fjord in what is referred to as the Estuarine circulation. An opposite elevation of the pycnocline at the bottom of the brackish layer neutralize this force for the underlying water. A gradual mixing at the pycnocline by entrainment and other various interactions supply salt to the brackish layer out the fjord, hence it becomes more salty. In deep waters as the Hardangefjord, the water to compensate for the mixing of more saline water into the brackish layer will come as a vertical flux [Aure, 2011].

For the Hardangerfjord the supply of fresh water has an annual mean of about 400 m^3/s. The supply normally reaches its maximum during June, while it is considerably less during the winter months [Ervik et al., 2008]. The large amount of fresh water supplied to the fjord leads to a maximum extent of the brackish layer during summer, typically reaching out to between section H6 and H7 (Figure 1.3) [Ervik et al., 2008]. A supply of 400 m^3/s fresh water to the fjord, leads to a transport of about 1800 m^3/s brackish

water out the fjord in the top 4-5 m [Ervik et al., 2008].

The brackish layer can be seen to be about 5 m thick in Figure 2.2 in June 2008, but has been found to affect the water salinity down to 15-25 m [Svendsen et al., 1972-73]. During the winter months the salinity is generally much higher for the whole fjord [Ervik et al., 2008].

Wind affects the heat balance of the ocean, but also transfers energy to the water giving rise to currents, waves and vertical mixing in a fjord. Increased exchange of air over the water also contributes to increased loss of sensible and latent heat. The currents driven by the wind decrease logarithmic with depth. The direction of the current deflects towards the right of the overlaying water and wind (on the northern hemisphere). The depth where the wind no longer is notably, is called the Ekman depth. The Ekman depth and magnitude of the wind induced current is increasing with the strength and duration of the wind. A decrease in velocity with depth can be seen in relation to the stratification of the water. A strongly stratified water column might not transfer the energy from the wind to as great depths as for a well mixed case [Svendsen and Thomsom, 1978]. As the momentum gained from the wind still is the same, a greater velocity will occur close to the surface in the strongly stratified case. Topography will lead the wind in the along-fjord direction. Especially the inner part of the Hardangerfjord is surrounded by tall mountains leading to channelling of the wind. Further out the fjord, the landscape is more open, the wind is likely to greater variability in direction [Farmer and Freeland, 1983].

During periods of sustaining wind, the low density water close to the surface might be transported along with the wind. Close to a boundary the surface water might be removed or piled up, leading to up- or down-welling.

In the beginning of February 1972, up-welling was observed in Eidfjord in the inner part of the Hardangerfjord (Figure 1.1). Strong easterly winds (velocities reaching 15-20 m/s) led to a transport of surface water out the fjord, forcing denser and more saline water to rise to the surface at the head of

the fjord. Low air temperatures made the dense water even denser as it was being transported out the fjord. This lead to an unstable stratification and heavy mixing in the upper 25 meters of the fjord [Svendsen et al., 1972-73].

Due to the rotation of the earth, wind driven currents may be forced to deflect towards its right (Ekman drift)[Cushman-Roisin et al., 1994]. This happens both inside the fjord and regularly along the coast. When the water is stratified, up- and down-welling cause a displacement of the pycnocline which may generate internal waves. Sundfjord [2010] showed internal pulses generated by wind drive up-welling along the coast to enter the Hardangerfjord regularly causing an exchange of 40-80% of the water in the upper 11 m for the region outside section H6 (Figure 1.3).

Tides. Whereas the parameters mentioned above mostly affects the hydrography close to the surface, the tides affects the whole fjord moving a water column back and forward. According to Ervik et al. [2008] the semi diurnal component M2 is dominating in the Hardangerfjord, leading to tides having a mean amplitude of 0.6 m. This causes a transport of 30 000 m^3/s at section H7 close to the mouth of the fjord (Figure 1.3) [Ervik et al., 2008]. Since the fjord is a closed basin the tidal wave is reflected at the head causing a standing wave, with decreasing velocity close to the head. Thus, the current velocities associated with the tidal wave are generally modest in fjords except for narrow or shallow parts. Tides renews water in the fjord by replacing lower density water behind the sill, but also feeds turbulent mixing with energy behind constrictions (Pond and Pickard [1983]). Tides may also cause internal waves in vertically stratified fjords generated at sills or straits [Stigebrandt, 1980]. Internal waves, generated both by wind driven up-welling or tides, is a source of vertical mixing in a fjord [Pond and Pickard, 1983]. The tides as a transport mechanism for water is limited since the net unidirectional flow only lasts for 5 to 6 hours before reversing.

The Coastal water variability. Water exchange in the fjord is highly affected by the conditions outside the fjord. Fresh water run off from land mixes

with Atlantic water at the coast resulting in the Norwegian Coastal Current (NCC) passing right outside the mouth of the Hardangerfjord [Sætre, 2007]. The NCC is driven northwards by the density difference between less saline water close to land and the saltier water influenced by the Atlantic water. The wind conditions in the area may both decrease the NCC, accumulating the water at the coast (Ekman drift) [Gade, 1986] and make the transportation northwards more efficient. Northerly winds, which often is dominating during summer along the Norwegian coast, will cause an Ekman drift away from the coast, lifting the underlying Atlantic water making penetration of water into the fjord possible due to the pressure differences. The exchange of water in the fjord may be partial or full, depending on the density difference and the period of time the exchange is possible. In the winter southerly winds are dominating. The Ekman drift accumulates coastal water at the coast, making water penetrating into the fjord more difficult.

The atmospheric circulation in the North Sea region, bringing cyclones and anti-cyclones towards the Norwegian coast, creates variations in the wind at a much smaller time scale than seasonal. Winds persisting 2-5 days is enough to change the pressure field at the coast and flush the entire upper layer of a typical Norwegian fjord [Sætre et al., 1988].

Bathymetry is important since it both steers currents and increase the turbulent mixing of the water. Undisturbed currents prefer to follow the isobaths [Pond and Pickard, 1983]. Narrows, sills and straits hinder the currents which often leads to an increase in velocity [Pond and Pickard, 1983]. At the lee side of the narrows, eddies are often created, leading to an increase in turbulence in the fjord [Farmer and Freeland, 1983]. The topography can both generate and break internal waves and hence release energy available for turbulent mixing [Farmer and Freeland, 1983].

Rotational motion of the water masses, due to the Earth's rotation, can be expected to be observed in areas where the width of the fjord is of the same scale as the Internal radius of deformation (R) or larger [Gill, 1982].

Equation 2.2 gives the Internal radius of deformation for a fjord with a two-layer system, where the upper layer is thin compared to the lower layer.

$$R = \frac{\sqrt{g'H}}{f} \tag{2.2}$$

The Internal radius of deformation is given in Equation (2.2) where g' is the reduced gravity expressed as $g' = \frac{g \triangle \rho}{\rho}$. g is the gravity constant, $\triangle\rho$ is the density difference between two layers of water, ρ is a typical reference gravity, H is the depth of the water and f is the Coriolis parameter given as $f = 2\Omega \sin \varphi$ where Ω is the rotation rate and φ the latitude of the earth.

Typical values for the Hardangerfjord area are of order of magnitude: $g = 10[m/s^2]$, $\triangle\rho = 10[kg/m^3]$, $\rho = 10^3[kg/m^3]$ which gives a reduced gravity, $g' = 10^{-1}[m/s^2]$. As the rotation of the Earth is $\Omega = 7.3 * 10^{-5}[radians/sek]$ and the Hardangerfjord is placed aproximately at $\varphi = 60°$ the Coriolis parameter becomes $f = 1.4 * 10^{-3}[s^{-1}]$. Combining the reduced gravity, the Coriolis parameter and the depth $H = 10^2[m]$, we find the Internal radius of deformation of the Hardangerfjord to be about 3 km. Hence we expect only the part of the fjord less than 1 km wide to be unaffected by rotational dynamics. This indicates that rotational motion of the water is expected to occur in most parts of the Hardangerfjord.

2.2 Life cycle and behaviour of the Salmon louse

The salmon louse *(Lepeophtherius salmonis)* life cycle consists of ten stages after hatching. During the two first stages (nauplius stages), the salmon lice is planktonic and non feeding. After the two nauplius stages, it reaches a copopodite stage, still planktonic. In order to survive the next seven stages it needs to find a host to feed on during this third copepodite stage [Johnson and Albright, 1991a]. If finding a host, it normally stays on this host, eating

its mucus and skin in seven more development stages [Heuch and Karlsen, 1997]. However, to find a salmon or sea trout to live on, the salmon louse needs to be transported by the currents to a close proximity. This thesis focuses on the dispersion of salmon lice during the three first planktonic stages.

The development of the louse has been shown in laboratory experiments to vary both with salinity and temperature. Johnson and Albright [1991b] found the time to hatching to take 17.5 days at 5°C, 8.6 days at 10°C and 5.5 days at 15°C. The time from hatching to the copepodite stage, takes between 1.9 to 9.3 days (at 15°C and 5°C). Both the egg-development time and especially the time from hatching to the infectious copopodite stage, found by Johnson and Albright [1991b], correspond well with the development times found by others [Stien et al., 2005] shown in Figure 2.3. The symbol ■ in Figure 2.3 are Johnson and Albright [1991b] results, whereas the other symbols are results from other experiments.

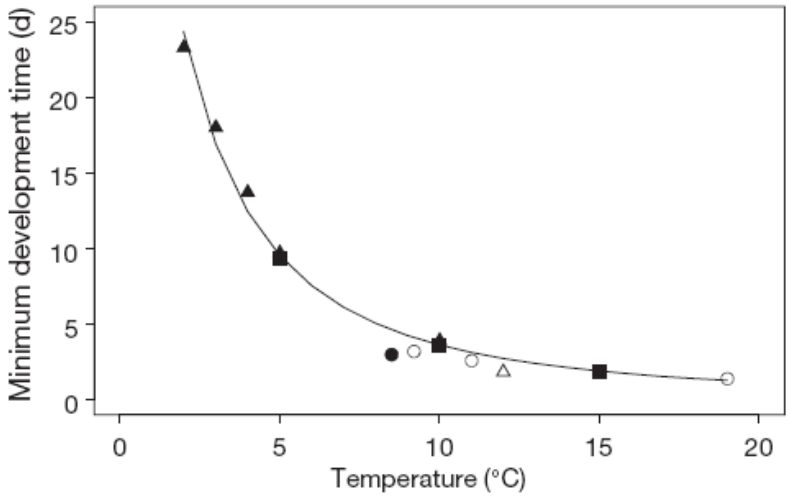

Figure 2.3: *Minimum time of duration of the first two nauplii stages. Figure from Stien et al. [2005]*

The development time of the nauplii stages (Figure 2.3) seems, at least for temperatures within the range $2 - 20$°C, to follow the regression line in

Equation (2.3):

$$time = \frac{\beta_1}{(T - 10 + \beta_1\beta_2)^2} \tag{2.3}$$

Here $\beta_1 = 24.7(\pm 1.43)$, $\beta_2 = 0.525(\pm 0.017)$ and T is the water temperature (Stien et al. [2005]). It can be seen in Figure 2.3 that the time from hatching to the infectious copepodite stage is about 50 degree days. Thus this approximate is used as duration of the first two nauplii stages in the salmon lice model (Chapter 2.4).

A clear correspondence between temperature and survival time has not been found for the salmon lice during its copepodite stage [Stien et al., 2005], but long development time due to low temperatures are assumed to increase the mortality. The maximum survival time for a copepodite, unable to find a host, was found to be 17 days at 10°C and a salinity of 25 [Johnson and Albright, 1991b]. However the average survival time was considerably lower, between 2 - 8 days. Bjørn et al. [2011] found the survival time of the infectious copepodite stage to be around 100 degree days. This is the time used in the salmon lice model. After the infectious copepodite stage lasting 100 degree days it is assumed that the lice are dead or have found a host. Either involves a non infectious lice.

No hatching occurred in laboratory experiments for salinity less than 15, and active nauplii and copopodites were not obtained for salinity less than 20 [Johnson and Albright, 1991b]. Both hatching and development to copepodite stage have been found at low temperatures [Boxaspen and Næss, 2000] the result seen as ▲ in Figure 2.3. Down to 2°C Boxaspen and Næss [2000] found all but one pair of eggs to hatch, and most eggs developed to copopodite at temperatures above 4°C.

The salmon lice have during its copepodite stage shown a diurnal migration pattern in laboratory experiments, swimming upwards towards the

surface exposed to light, and spreads out downwards if no light [Heuch et al., 1995]. Observations done by Bengtsen [2011] confirm this. Though Johnson and Albright [1991b] did not find nauplii able to swim, Heuch et al. [1995] made observations suggesting diurnal migration also for the nauplius stage, although at a notably smaller extent than for the copepodite.

In experiments exposing copopodites to a salinity gradient (both step and linear) the copepodites seemed to avoid salinity under 20, with no total absence [Heuch, 1995]. When exposed to light, the copepodites accumulated at a salinity of 20, being more spread out during the experiments in the dark. This seems to coincide with Johnson and Albright [1991b] observation of no active nauplii and copepodites developing at salinities less than 20. Experiments executed by Bengtsen [2011] found salmon lice at all salinities down to 10 in a salinity gradient experiment. Where Heuch [1995] found the number of louse to increase with increasing salinity, Bengtsen [2011] suggest that this is a result of too steep salinity gradient, where the salmon lice avoids rapid changes rather than low salinities due to osmoregulating [Bengtsen, 2011].

2.3 The fjord model

Currents, temperature, salinity and other parameters was simulated with the Regional Ocean Model System (ROMS) for the Hardangerfjord area (Figure 1.2) during the period 15th of April to 31st of June. ROMS solves the primitive equations for conservation of momentum, temperature, salinity and mass in order to obtain a detailed description of the hydrography in the fjord.

The parameters are simulated having a temporal resolution of 10 seconds, but are written out every hour. The external forces (as wind, temperature and fresh water input) used by ROMS have a resolution of 6 hours, or less. They are all linearly interpolated to give ROMS hourly updates at the boundary.

The bathymetry for the simulated area was provided by the Norwegian

Mapping Authority (Statens kartverk). The area was divied into 994 × 440 grid nodes with 200 m × 200 m horizontal resolution. The primitive equations were solved using a staggered Arkawa C-grid [Albretsen et al., 2011].

Vertical s-coordinates were used, following the terrain for depths deeper than a critical depth and equally spaced if shallower [Albretsen et al., 2011]. The vertical is divided into 35 layers, where the 35th layer is the surface. This gives a resolution of 14 to 34 grids in the top 15 meters depending on the total depth at the location. Shallower water gives more grid nodes in the surface layer due to the stretching. The maximum depth has been set to 400 m in order to speed up the computations and the bathymetry was smoothed in order to obtain numerical stability over steep slopes. The real maximum depth in the Hardangerfjord more than doubles the models maximum depth, exceeding 800 m in the inner part. The results from these set-ups can not be used to examine the deep water circulation in the fjord, but it is assumed to give reasonable good results for the upper 100 m which is of interest for the problem at hand.

2.3.1 External forcing

Atmospheric input The atmospheric boundary conditions are produced by the European Centre for Medium-Range Weather Forecasts (ECMWF). The ECMWF Re-analyses (ERA-Interim) fed into ROMS have a resolution of 0.7 °. This corresponds to approximately 70 km. Cloud cover, wind, temperature, pressure and humidity at the surface was extracted from ERA-Interim and fed into ROMS 4 times a day (00, 06, 12 and 18 UTC) and accumulated precipitation twice a day (00 and 12 UTC). ROMS calculates both short and long wave radiation terms internally.

Input along external boundaries IMR has done ROMS simulations of 800 × 800 m horizontal resolution covering the Norwegian coast [Albretsen et al., 2011]. Data from this model (velocities, turbulent parameters, sea surface elevation, temperature and salinity) were nested to 200 m scale using

linear interpolation, and used as input to the fjord model 4 times a day (00, 06, 12, 18 UTC).

Fresh water input Fresh water input from about 100 rivers were put into the model using results from a data driven hydrological model developed by the Norwegian Water Resources and Energy Directorate (NVE) [Petterson, 2008] and [Sandvik, 2010-2011].

Tidal input Tidal forces were applied based on results from the barotropic model TPXO7.2. The data is downscaled and preprocessed to match the modelled time enabeling the fjord model to simulate 4 realistic tidal constituents [Albretsen et al., 2011].

2.3.2 The governing equations

The governing equations solved by ROMS are here presented using Cartesian coordinates (myroms.org [2011]). The variables are explained in Table 2.2.

Table 2.2: *Description of the variables used in the governing equations*

D_u, D_v, D_T, D_S	Diffusive terms
F_u, F_v, F_T, F_S	Forcing terms
f	Coriolis parameter
g	acceleration due to gravity
P	Total pressure
$\rho_0 + \rho(x, y, z, t)$	Total *in situ* density
$S(x, y, z, t)$	Salinity
$T(x, y, z, t)$	Potential temperature
t	Time
x, y	Horizontal coordinates
z	Vertical coordinates
u, v, w	(x, y, z) components of vector velocity $\overrightarrow{v}$

The horizontal momentum is conserved following from Newtons 2nd law.

$$\frac{\partial u}{\partial t} + \overrightarrow{v} \cdot \bigtriangledown u - fv = -\frac{1}{\rho_0}\frac{\partial p}{\partial x} + F_u + D_u \tag{2.4}$$

$$\frac{\partial v}{\partial t} + \overrightarrow{v} \cdot \bigtriangledown v + fu = -\frac{1}{\rho_0}\frac{\partial p}{\partial y} + F_v + D_v \tag{2.5}$$

The Boussinesq approximation has been used, neglecting density variations except the vertical directed buoyancy force. The pressure gradient is then given by:

$$\frac{\partial p}{\partial z} = -\rho g \tag{2.6}$$

For an incompressible fluid the volume is conserved as follows:

$$\frac{\partial u}{\partial x} + \frac{\partial v}{\partial y} + \frac{\partial w}{\partial z} = 0 \tag{2.7}$$

The salinity and temperature is determined by the conservation of salt and temperature in the following equations:

$$\frac{\partial S}{\partial t} + \overrightarrow{v} \cdot \bigtriangledown S = F_S + D_S \tag{2.8}$$

$$\frac{\partial T}{\partial t} + \overrightarrow{v} \cdot \bigtriangledown T = F_T + D_T \tag{2.9}$$

The density is calculated by using an equation of state involving temperature, salinity and pressure:

$$\rho = \rho(T, S, P) \tag{2.10}$$

2.4 Salmon lice growth and advection model

The salmon lice growth and advection model is a modified version of a Lagrangian Advection and DIffusion Model (LADIM) which has been developed

and used at IMR for about 20 years [Ådlandsvik and Sundby, 1994]. Hourly values of simulated currents, salinity and temperature from ROMS are used by the salmon lice model. LADIM uses the resolution from ROMS (see Chapter 2.3),while linearly interpolating the velocity, temperature and salinity both vertically and horizontally to the sub-grid position. Particles were released hourly at 12 positions (Figure 3.9) during the time period given in Table 1.1.

Salmon lice characteristic included in the model is diurnal migration and growth as degree days.

LADIM simulates particles swimming up during daytime and down during night, to simulate salmon louse behaviour found in experiments (Chapter 2.2). The temporal resolution was set to 180 seconds to make a valid interpolation based on the ROMS models resolution and velocities. Output from the salmon lice model with information of the particles position, age, temperature and salinity were given every hour.

LADIM calculates light using time of year and latitude. This was used to give the particle an upwards velocity of $3 * 10^{-4}$ m/s when exposed to daylight. This velocity corresponds to a vertical displacement of almost 13 m over 12 h. In the dark the particles get the same velocity downwards. The resulting diurnal migration pattern is shown in Figure 2.4. Experiments have shown copepodids to have a mean velocity of $1.55 * 10^{-3}$ m/s in an undisturbed system and $1.7 * 10^{-2}$ m/s when stimulated by vibrations [Heuch and Karlsen, 1997]. It can be seen that none of the velocities used in the model exceeds swimming velocities found in experiments. The particles was given a horizontal and vertical random walk within the range of $< -0.015, 0.015 >$ and $< -10^{-5}, 10^{-5} >$ m/s, normally distributed around 0 . The vertical random walk was applied to simulate the randomness of lice distribution observed in laboratory experiments [Heuch, 1995]. The age of a copepodite was set to 50-150 degree days [Bjørn et al., 2011].

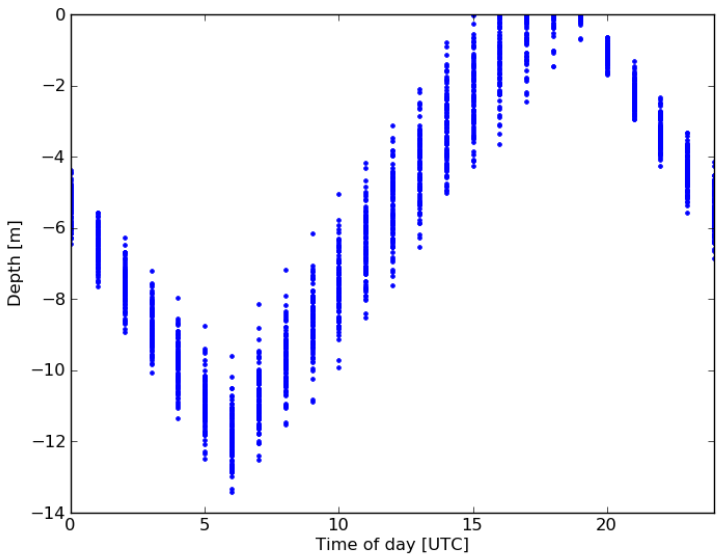

Figure 2.4: *Positions of the lice illustrating the vertical migration of 100 lice due to daylight*

Both Johnson and Albright [1991b] and Heuch [1995] results from laboratory experiments indicate that salmon lice avoid water with salinity under 20. However, newer results indicate that salmon louse may stay in less saline water if given time to adjust their inner salt level [Bengtsen, 2011]. The potential avoidance of low salinity water will only come into account for limited areas of the fjord close to the head. No action was therefore taken for the simulated lice to avoid less saline water.

Seaward migrating post-smolt have, using acoustic transmitters, been shown to swim close to the surface [Thorstad et al., 2004] and [Gudjonsson et al., 2005]. Measurements done at different light intensities in the Hardangerfjord showed no post-smolt migrating out the fjord at greater depth than 6.5 m [Davidsen et al., 2008]. Only lice close to the surface is simulated (released at 5 m depth). This is the depth at which they are a potential threat to the wild salmon migrating out the fjords.

CHAPTER 3

Results

3.1 Currents

3.1.1 Observations with the Acoustic Doppler Profiler (ADP)

Three Acoustic Doppler Profilers (ADP) measured the current at the positions ADP4, ADP5 and ADP6 (Figure 1.3) in the Hardangerfjord during the spring and summer of 2007. The measurement of currents will be used both to describe the circulation of the fjord and to evaluate the numerical model results used to simulate the dispersion of salmon lice. An evaluation of the simulated currents, temperatures and salinity, as the driving forces of the modelled lice, will be done in Chapter 4.1.

ADP4 is placed in the main artery of the Hardangerfjord (Figure 1.3). The instrument cannot measure all the way from the depth to the surface due to side-lobbing of the angled sound beams. We lose a distance equal to 10% of the instrument depth from the surface and downwards. The data is

not smoothed in any way, and both tides and currents of longer duration can be seen (Figure 3.1).

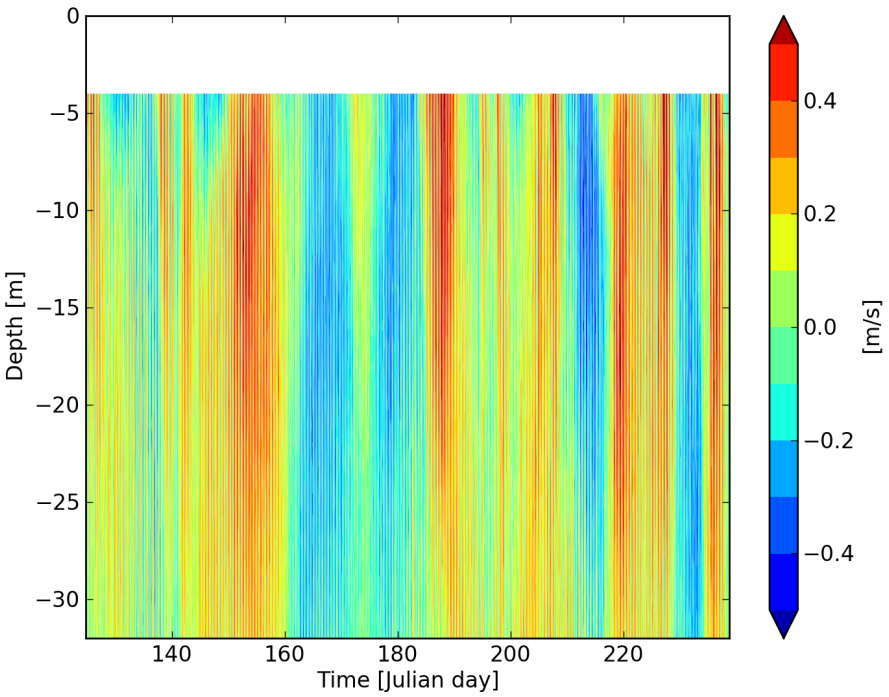

Figure 3.1: *Along-fjord current component observed at position ADP4. Positive values gives current directed along compass direction* 30°*, into the fjord.*

Figure 3.2 shows time series at 18 m depth of the current from ADP4 along with ADP5 and ADP6 (see Figure 1.3 for position). The currents are decomposed to the dominating direction. Positive currents are directed into the fjord, along compass direction given in Table 3.1. The currents are smoothed with a 24 hour time filter to eliminate tides.

Table 3.1: *Compass direction of dominating current and instrument depth.*

Station	Positive direction	Depth
ADP4	30°	33 m
ADP5	105°	18 m
ADP6	110°	58 m

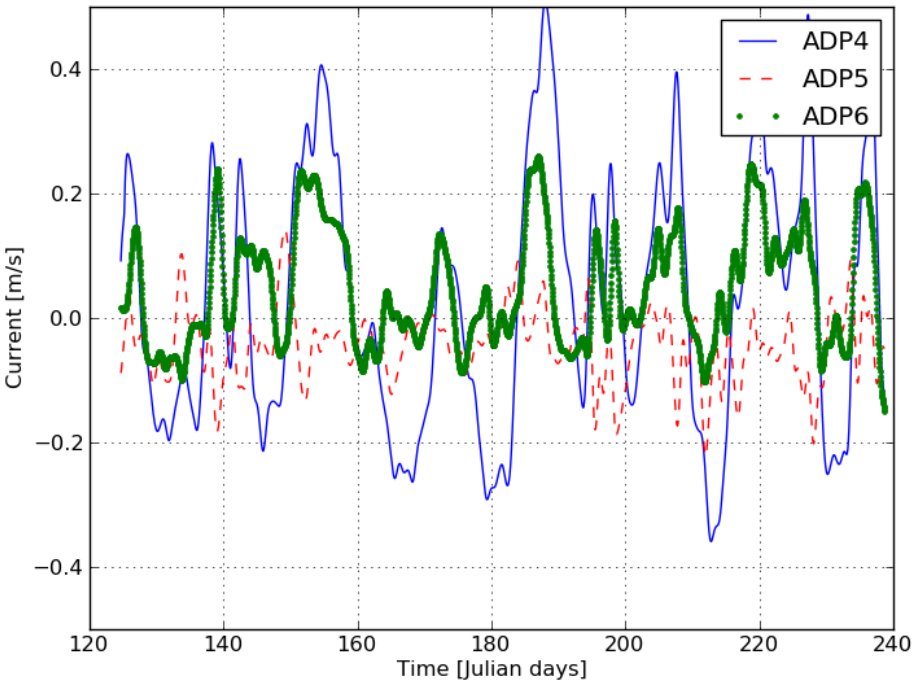

Figure 3.2: *Along-fjord current components at 18 m depth for ADP4-6. Positive values are into the fjord*

Both ADP4 and ADP6 seems to measure the same current but the magnitude at ADP6 is less than at ADP4. The current at ADP5, located closer to ADP4 than ADP6, does not have the same long lasting current periods. It also shows weaker currents and has more fluctuations. ADP5 and ADP6 are opposite directed at several occasions, indicating rotational motion between

them, or a recirculation pattern. This also seems to occure most frequently during periods when ADP4 show strong currents directed into the fjord (Figure 3.2).

3.1.2 Fjord model

The very limited current measurements in the Hardangerfjord, only 3 in the entire fjord this specific year, makes information from numerical models of crucial importance in order to make a detailed description of the salmon lice dispersion in the fjord. The observed currents show periods lasting for several days with continous flow into or out of the fjord (Figure 3.2). Whereas tidal currents move water, and hence lice, backwards and forwards and in sum not very far, strong currents of long duration can potentially transport salmon lice great distances. Long continuously currents may be generated directly by wind, or indirectly by internal waves generated at the coast. Pulses of strong currents entering the Hardangerfjord regularly have earlier been shown to be internal waves generated at the coast [Sundfjord [2010]; Asplin et al. [1999]]. Results from the numerical fjord model are useful in order to examine how these long lasting currents propagate into the fjord. It may also describe the fluctuating currents measured between ADP5 and ADP6.

Simulated volume flux through the top 15 m in the sections in Figure 3.3, was calculated in order to give a more thorough description of the movement of the water masses.

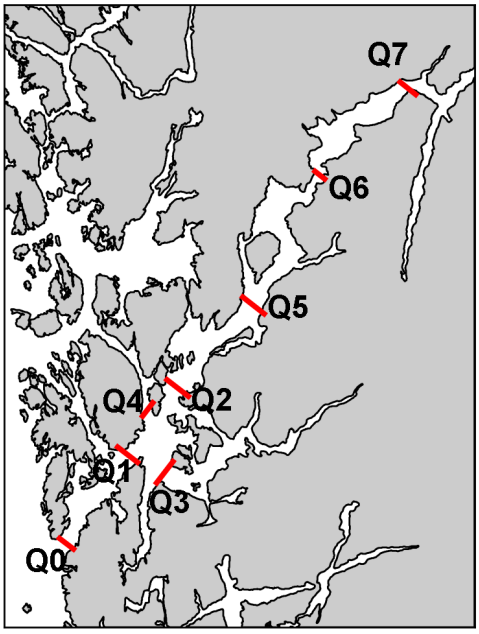

Figure 3.3: *Sections (red lines) where the volume flux of the upper 15 m of the fjord has been extracted from the numerical model results.*

Positive values are flux into the fjord (to the north east), except for Q3 and Q4 where positive flux is towards north-west. That the water flux through Q3 and Q4, directed along the main branch of the fjord are smaller than the flux through Q1 and Q2 across the main branch of the fjord. Q3 and Q4 are opposite directed of Q1 and Q2 most of the time, illustrating that rotational motion is applicable here.

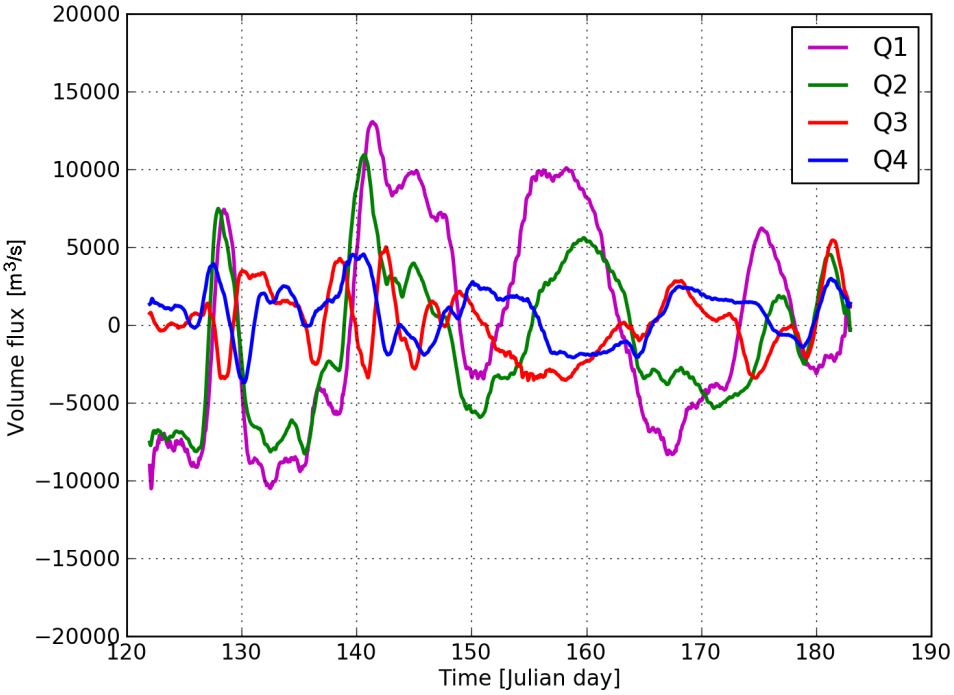

Figure 3.4: *Volume flux in the upper 15 m through the sections Q1-Q4 in the spring 2007 from the numerical model.*

The positive volume flux through section Q1, Q2, Q5, Q6 and Q7 are plotted in Figure 3.5.

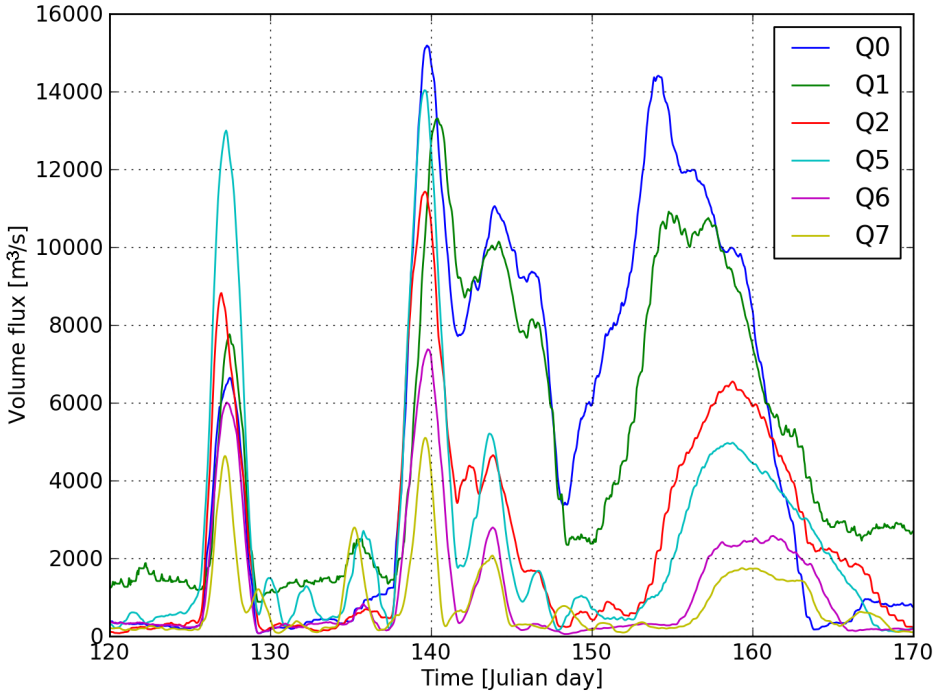

Figure 3.5: *Volume flux into the Hardangerfjord through the sections Q1, Q2, Q5, Q6 and Q7 in spring 2007 from the numerical model.*

Large pulses of incoming water occur every 15 - 20 day during the simulated period. The signal can be seen all the way from the mouth (at Q1) to the cross-section 120 km into the fjord (Q7). Two cases are especially investigated as they appear differently. First the influx around 9th of May (Julian day 129) which is more or less a simultaneous event at at all sections, with the highest value at section Q5. The geographical distribution of the daily mean current field at 5 m depth at 9th of May as seen in Figure 3.6 shows a unidirectional flow along the main artery of the fjord. The part of the fjord south of the section Q3 does not appear to be affected by the strong up-fjord flow. In the days between Julian days 126 and 130 the ERA-Interim winds used to force the fjord model are directed straight into the fjord continuously and with a magnitude up to 7 m/s.

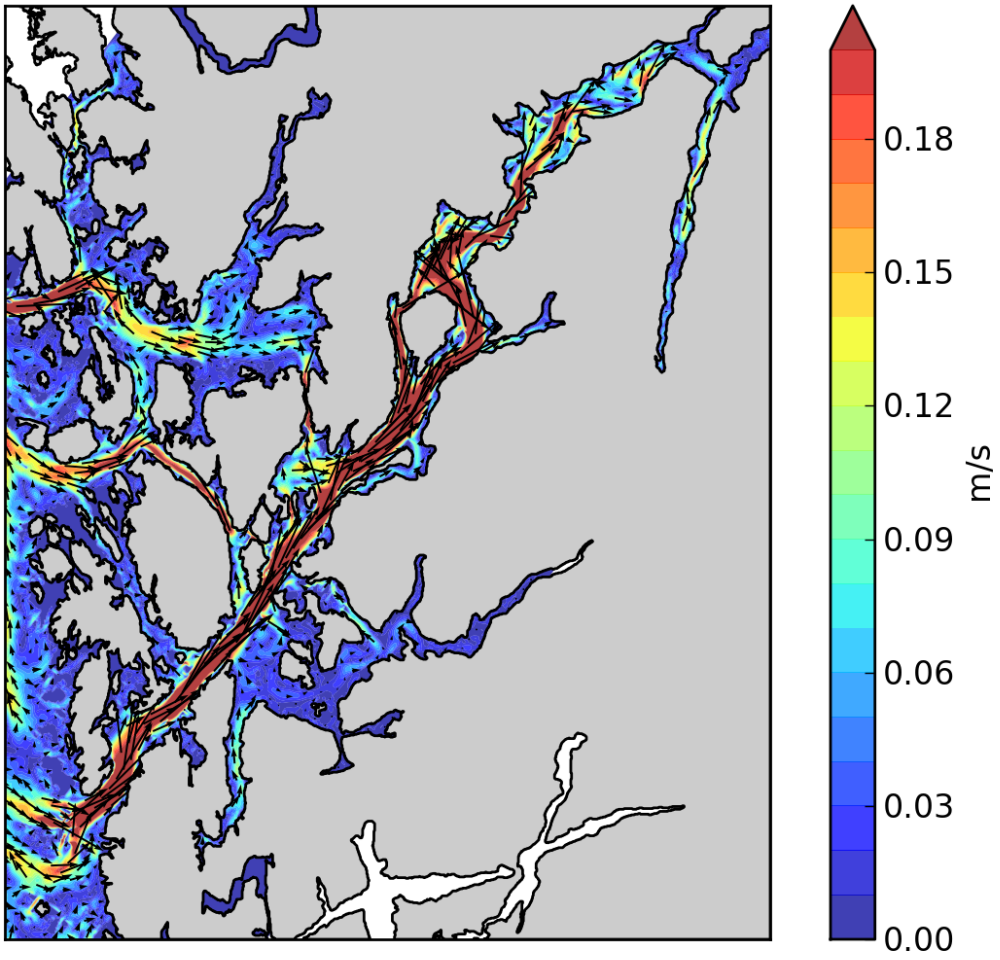

Figure 3.6: *Simulated current velocity (colours) and direction (arrows)at 5 m depth 9th of May (Julian Day 129), 2007*

The second case of inflow occur around 4th to 14th of June (Julian days 155 to 165) and is different from the previous episode (Figure 3.5). Now the volume flux of the upper 15 m is largest at the fjord mouth and decreases into the fjord. The peak volume flux is also delayed from the mouth and inwards indicating a propagating wave. The geographical distribution of

the current clearly shows how this wave propagate into the fjord (Figure 3.7 and 3.8). Inside of the section Q1 the current bends towards the south and hits the islands Halsnøy and Borgundøy. After about a days delay, the wave propagates further into the fjord. The propagation speed of the wave is approximately 0.23 m/s. The transport of water into the fjord during this period corresponds to ∼60% of the volume between section Q5 and Q6, and ∼10% between Q6 and Q7 accessible for water exchange in the upper 15 m. The winds used to force the fjord model are weak in this period, but three days prior to this pulse there was an episode of a southerly winds at the coast with speeds reaching 6 m/s. Such an event can produce a coastal down-welling and a subsequently internal wave [Asplin et al. [1999]; Sundfjord [2010]].

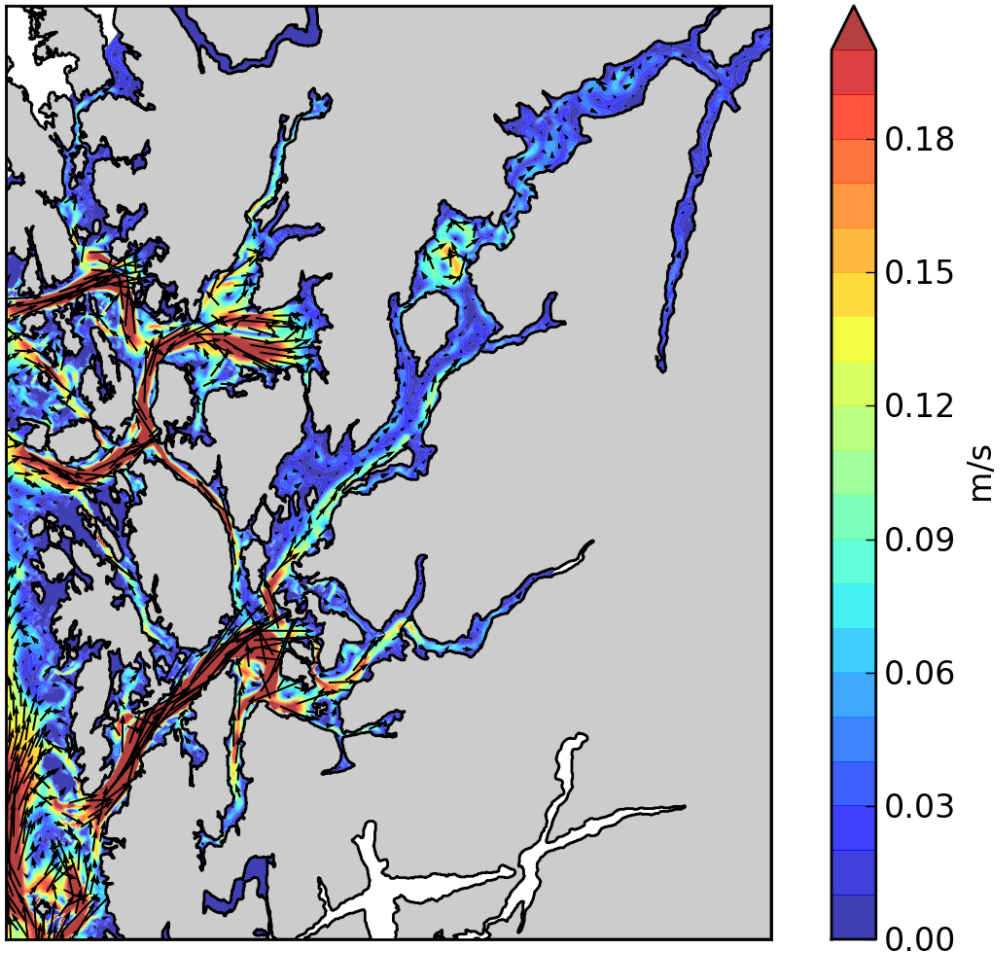

Figure 3.7: *Simulated current velocity (colours) and direction (arrows)at 5 m depth 6th of June (Julian Day 157), 2007*

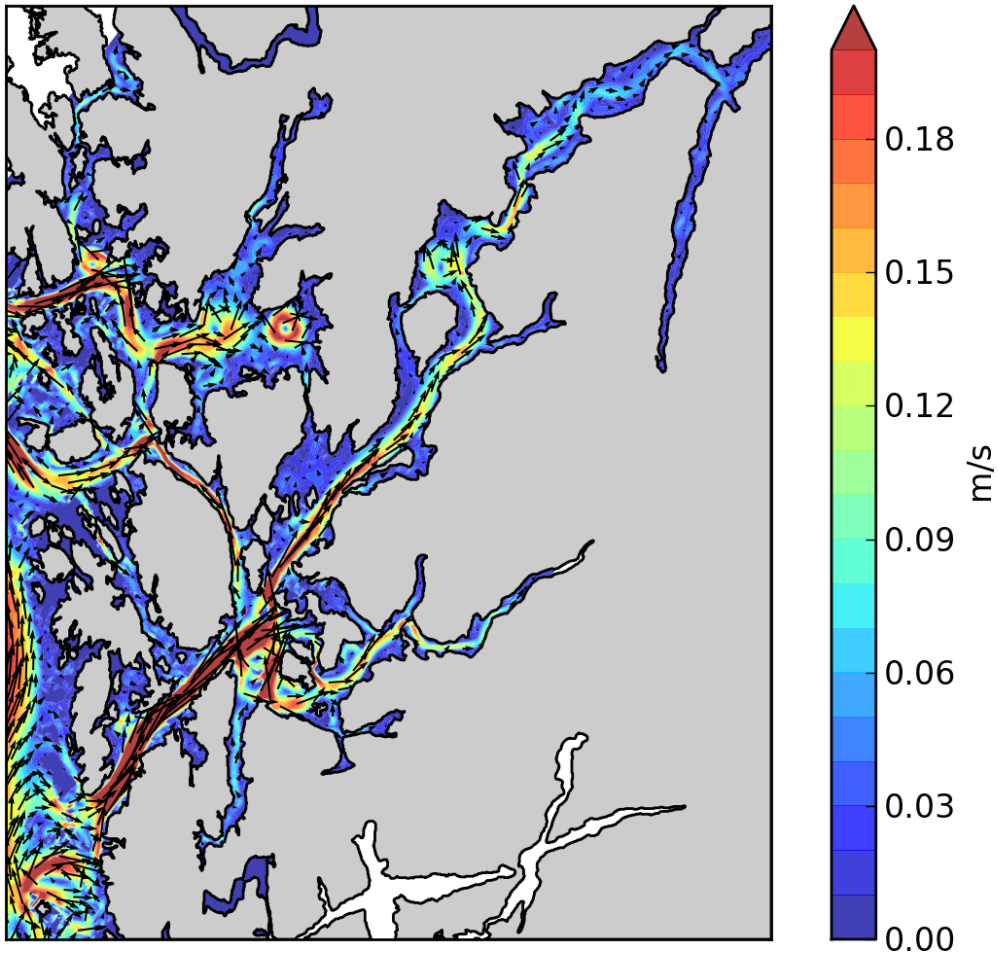

Figure 3.8: *Simulated current velocity (colours) and direction (arrows)at 5 m depth 9th of June (Julian Day 160), 2007*

3.2 Distribution of modelled salmon lice

Salmon lice advection and growth were simulated by the model for the period between 2nd of May to 9th of June (Julian day 122 to 160), 2007. The time period was chosen as this is typically when the post smolt migrates through the fjord towards the sea [Davidsen et al., 2008]. Twelve positions were used for particle, or model salmon lice, release (Figure 3.9). Two positions were outside the fjord and the rest distributed from the fjord mouth to head. The wide spread of the release positions in the fjord system reflects the actual distribution of salmon farms (Figure 3.10). At each release position, 100 particles were released hourly throughout the simulation. This is of course a huge underestimation of the total number of salmon lice released form e.g. a fish farm, however this number is sufficient to capture the variability of lice distribution and at the same time keeping the computing cost down.

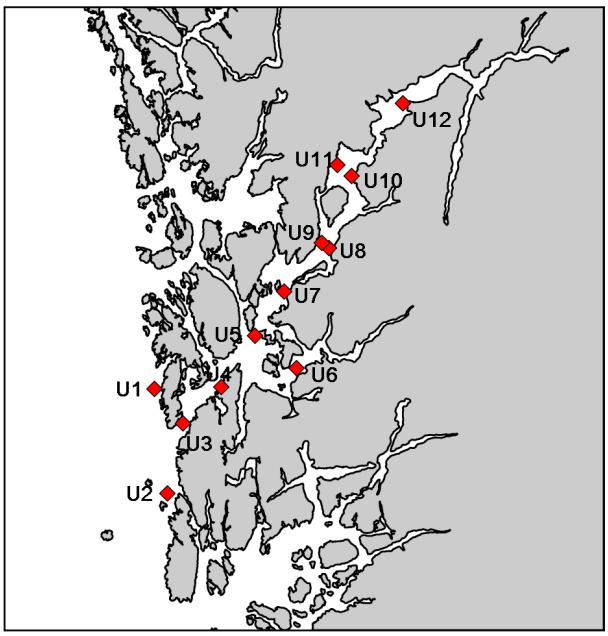

Figure 3.9: *Release positions of modelled lice*

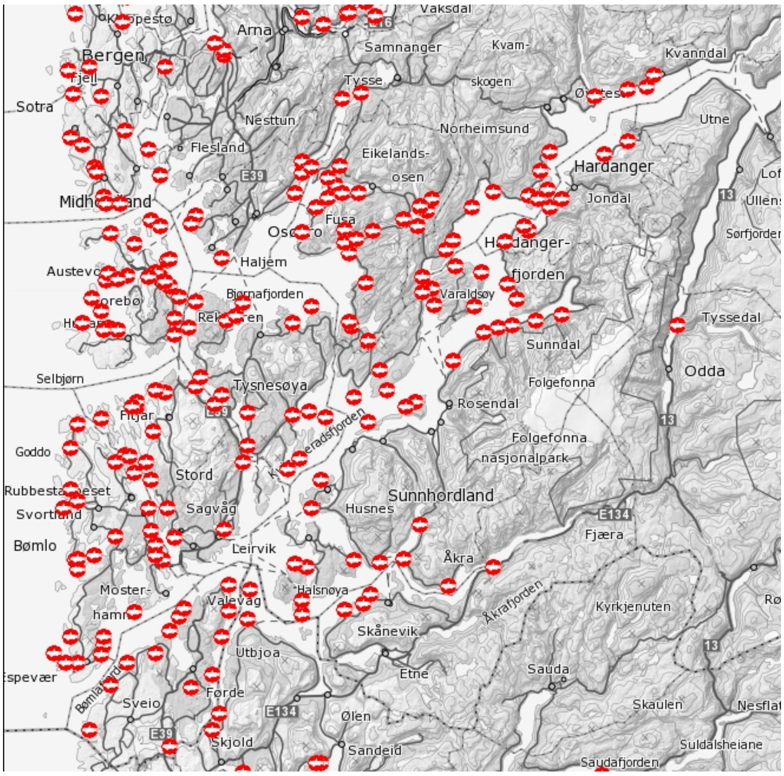

Figure 3.10: *Actual positions of fish farms (Directory of Fisheries [2011]).*

From the massive amount of results, only illustrating examples of different typical situations are presented. Since the currents used to drive the salmon lice model vary a lot in both time and space, the distribution patterns of salmon lice will also vary in the same way. The water temperature is close to 10 °C in the fjord for the simulation period, thus the lice will need 5 days to become infective. In all the examples the lice will be released at the position U4 and a total of 5 days advection is shown.

The first example (Figure 3.11) shows the advection of lice staring at 10th of May (Julian day 130). The currents are directed out of the fjord and the lice are being flushed offshore and spread out outside the fjord mouth after 5 days.

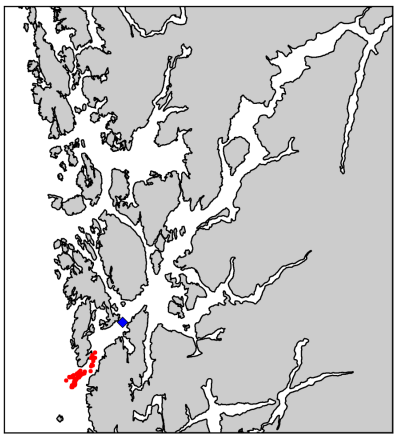

(a) *Particle positions after 1 day*

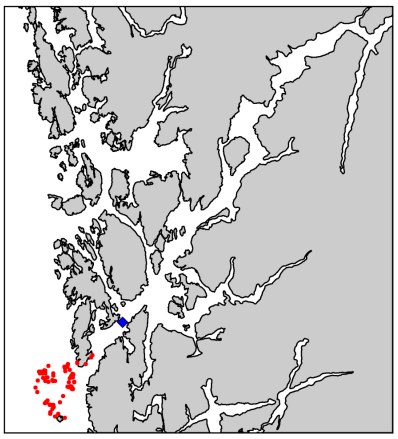

(b) *Particle positions after 2 days*

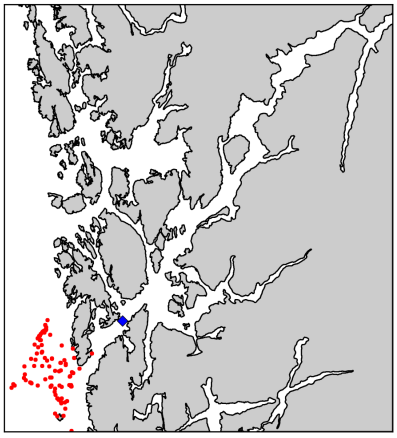

(c) *Particle positions after 3 days*

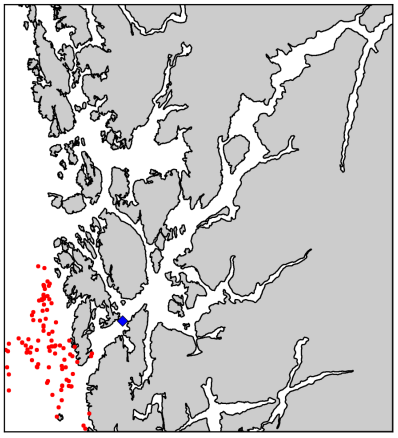

(d) *Particle positions after 4 days*

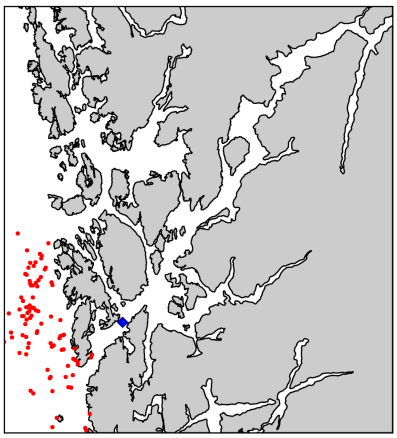

(e) *Particle positions after 5 days*

Figure 3.11: *Particle released at 10th of May (Julian day 130) at blue marker.*

In the second example (Figure 3.12) the particles are released the 18th of May (Julian day 138) and in the period with the along fjord wind event (Figure 3.5). In this case some of the particles stay closely to the release position, but the better part travel directly into the fjord. After three days most particles have covered a distance of more than 60 km which corresponds to speeds above 0.2 m/s. Both this example as well as the former show that the lice stay closely together being transported in a strong current and disperse as the velocities decrease.

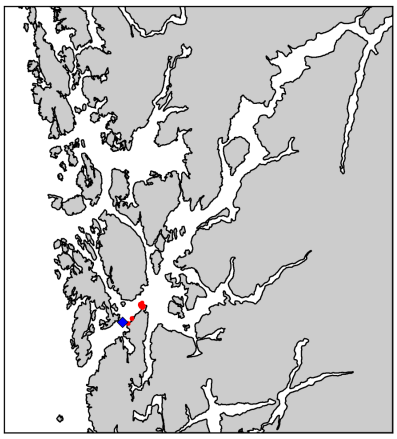

(a) *Particle positions after 1 day*

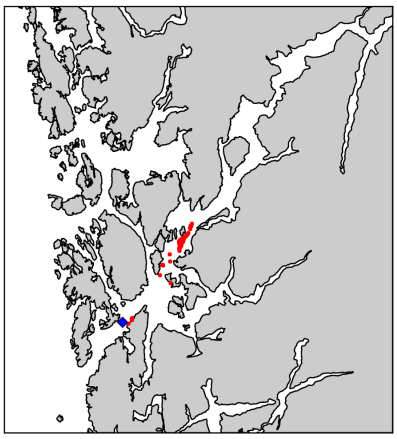

(b) *Particle positions after 2 days*

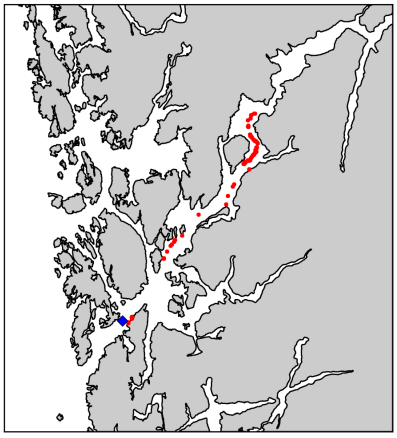

(c) *Particle positions after 3 days*

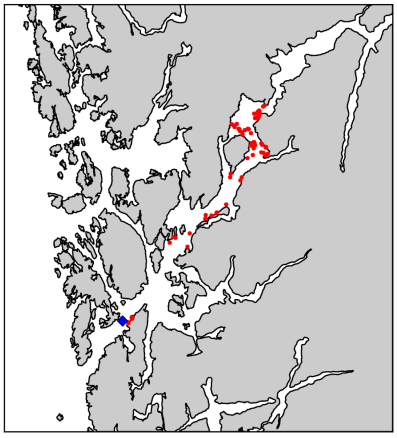

(d) *Particle positions after 4 days*

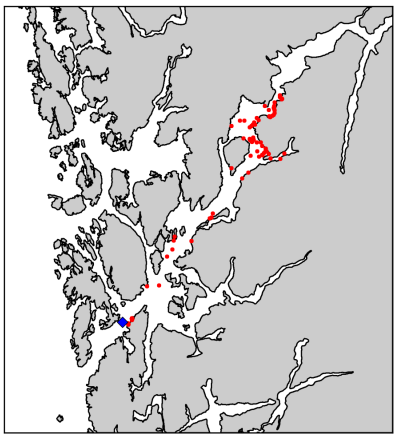

(e) *Particle positions after 5 days*

Figure 3.12: *Particle released at 18th of May (Julian day 138) at blue marker.*

In the final example (Figure 3.13) the particles are released the 3rd of June (Julian day 154) which is the period when the current is inwards but with the turn towards the south as seen in Figure 3.5. The particles are moved into the fjord along the northern fjord side before being turned to the south with the current and dispersed in the Halsnøy-Borgundøy area. Few particles continue southwards towards Skånevikfjorden, though.

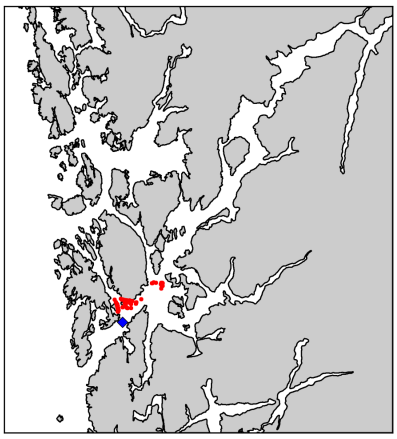

(a) *Particle positions after 1 days*

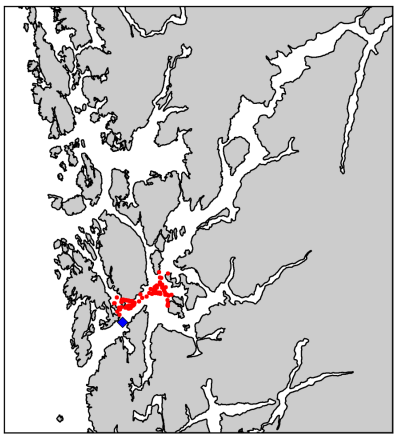

(b) *Particle positions after 2 days*

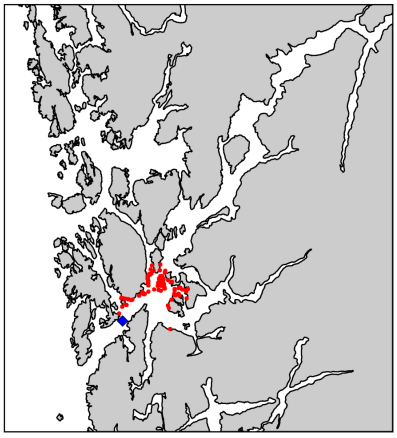

(c) *Particle positions after 3 days*

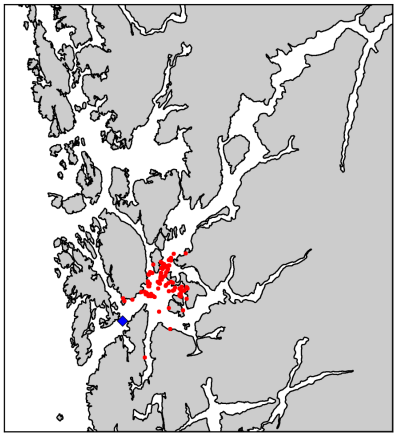

(d) *Particle positions after 4 days*

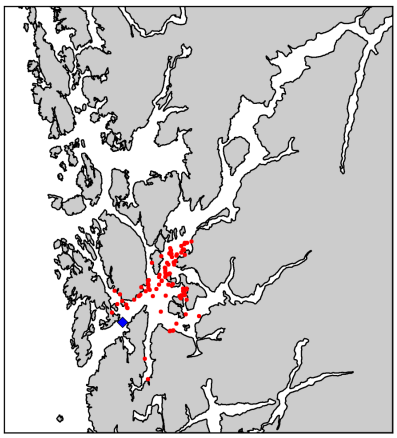

(e) *Particle positions after 5 days*

Figure 3.13: *Particle released at 3rd of June (Julian day 154) at blue marker.*

As shown, the variability of the lice dispersion can be large. Not shown are of course episodes of weaker currents and hence much less wide-spread distribution of the lice. The variations are great in both time and space, and it is necessary to construct an aggregated view in order to assess the area of influence by salmon lice from a specific location. In order to tell something about the actual infection pressure on salmonid fish during the simulation period, the number of infectious copepodids have been added up. The distribution of copepodids pr. unit volume for the whole simulation period from each of the release positions are presented in Figure 3.14.

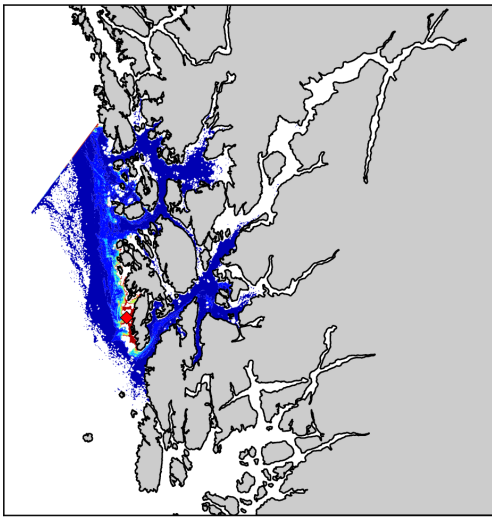

(a) *U1*

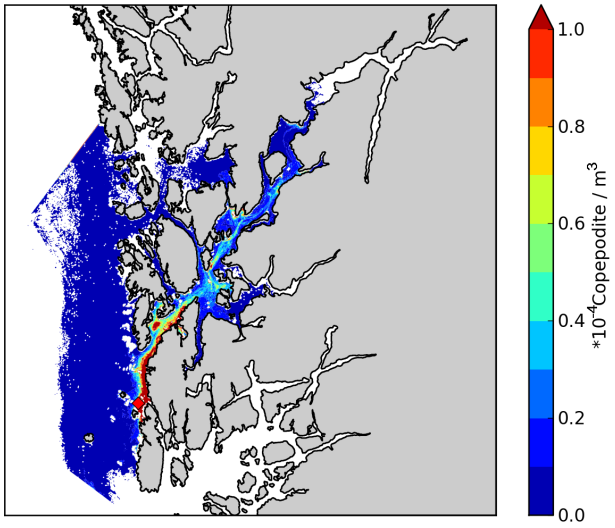

(b) *U2*

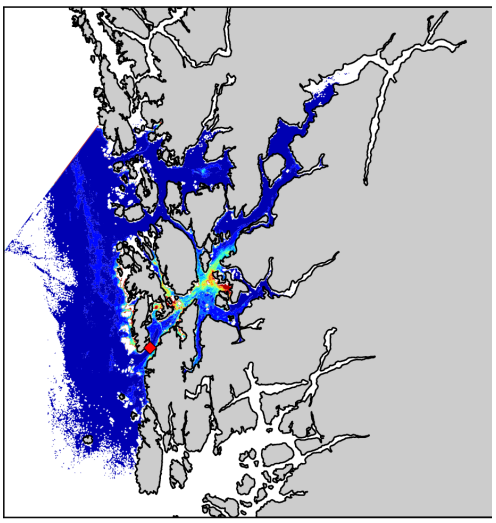

(c) *U3*

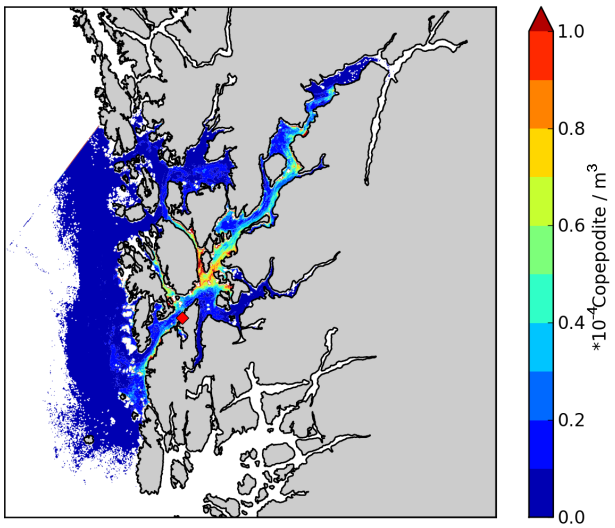

(d) *U4*

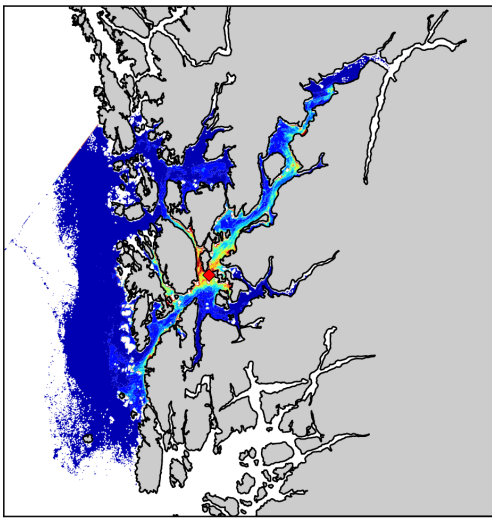

(e) *U5*

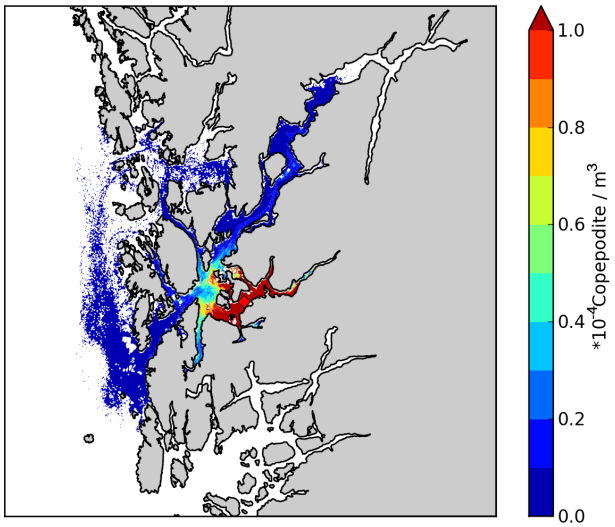

(f) *U6*

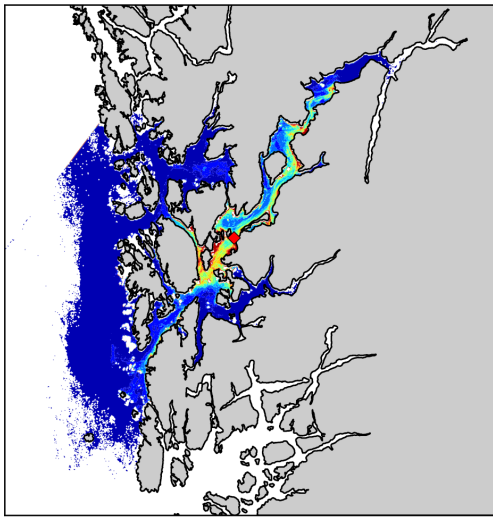

(g) *U7*

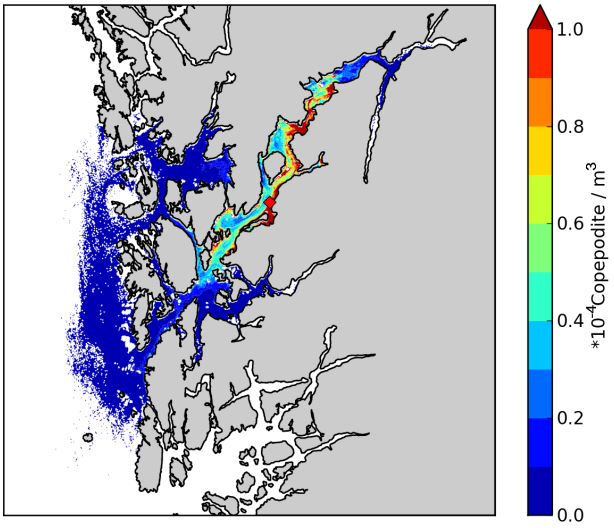

(h) *U8*

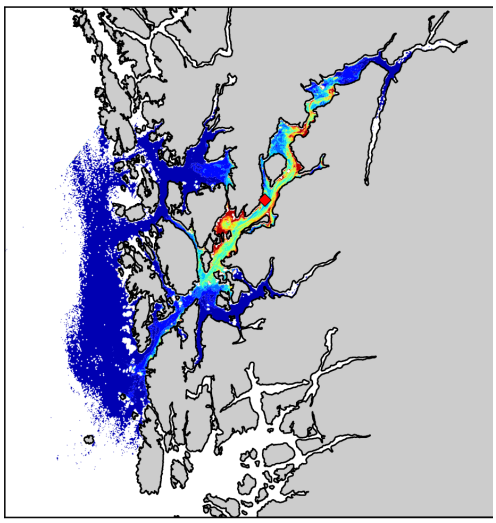

(i) *U9*

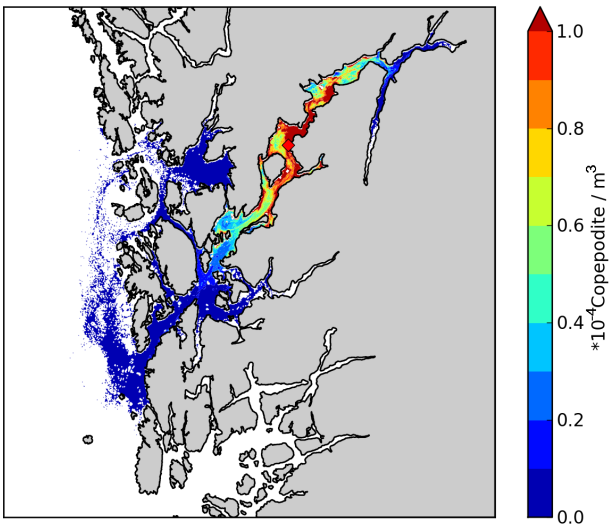

(j) *U10*

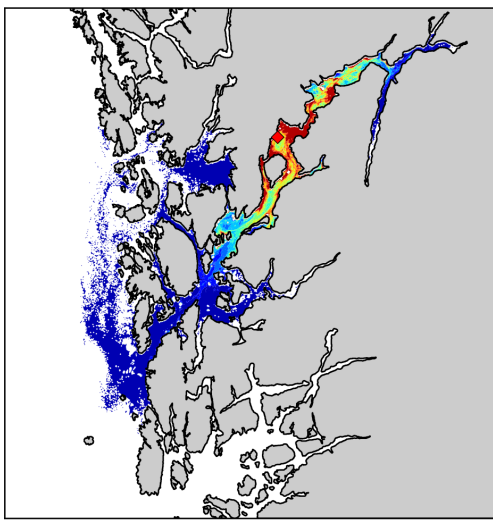

(k) *U11*

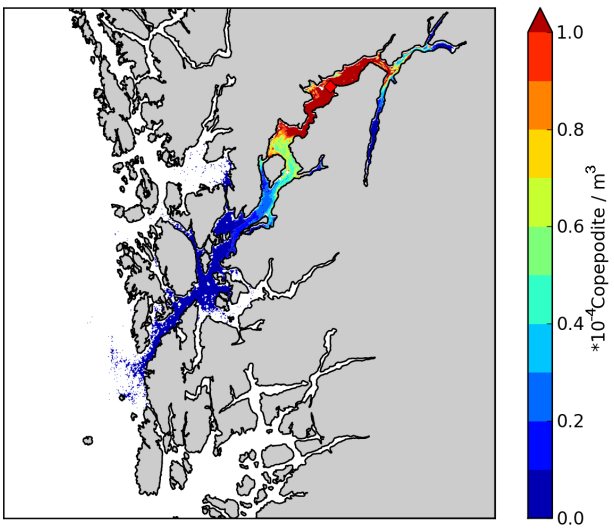

(l) *U12*

Figure 3.14: *Density plot of simulated lice during its infectious stage [Copepodite per Volume].*

The influence areas of infectious lice from all release positions are large, covering more or less the whole fjord one and each. In numbers the extension of the infectious areas are between 1300 and 4000 km^2. Lice from all positions except the innermost (U12) reach far outside the Hardangerfjord and into Bjørnefjorden to the north as well as to the offshore region (Figure 3.14l). As to the actual densities of lice, the variations are large. Even though a small number of lice are spread widely the high concentrations are found closer to the origins.The lice also seems to accumulate close to the shorelines, in narrows and in bays with potential large spatial variation.

The influence area for the lice released at the positions outside the fjord (U1 and U2) is concentrated to the fjord mouth and along the coast (Figure 3.14 a and b). For the release positions half way into the main fjord (U3, U4, U5 and U7) the lice are mainly concentrated in the central part of the fjord between ctd-sections H6 and H7 (Figure 3.14 c, d, e and g). In addition lice from the release position U7 reaches into the head areas of the fjord along with the lice from the release positions U8, U9 and U10 (Figure 3.14 g, h, i and j). The lice are mainly concentrated along the southern and eastern fjord sides. The lice released at U6 and U12 (Figure 3.14 f and l), i.e. the innermost positions in the Skåneviksfjord and the Hardangerfjord, have smaller influential areas compared to the lice from the other release positions, although even lice from these sources travel more than 100 km while still infective. The concentration of lice inside these smaller influential areas are thus higher.

The release positions U8 and U9 are only 2.5 km apart situated on each side of the fjord. The influential area of lice from these two release positions turns out to be different as the lice from U8 on the eastern fjord side mostly travel into the fjord and the lice from U9 on the western side of the fjord mostly travel out of the fjord (Figure 3.14 h and i). Lice form both positions accumulate along shores and create hot-spots of enlarged densities of lice. The release positions U10 and U11 are also placed on each side of the fjord, about 5 km apart. In this case the lice form influence areas that are relatively

similar (Figure 3.14 j and k).

CHAPTER 4

Discussion

4.1 Validation of the fjord model

Since the results from the salmon lice dispersion model depends heavily on the results from the fjord model, especially the current, it is necessary to validate the fjord model results. Model validation is no objective nor easy task [Dee, 1995], however it is still useful to be able to characterize the results at hand.

In the present case, observations of salinity and temperature at 8 cross-sections of the fjord and current at three locations (Figure 1.3) will be used for validation of the fjord model results. The temperature and salinity were measured twice during the simulation period, giving snapshots of the situation in the fjord during 7th to 8th of May and 8th to 9th of June. The observed currents represents time series overlapping the simulated currents for 56 days, hence most of the simulated period is covered.

4.1.1 Temperature and Salinity

Figure 4.1 and 4.2 shows observed and modelled temperature and salinity from a long-section of the fjord consisting of the middle stations at the cross-sections H1-H8. The model results are daily mean values for the comparable time.

Temperature

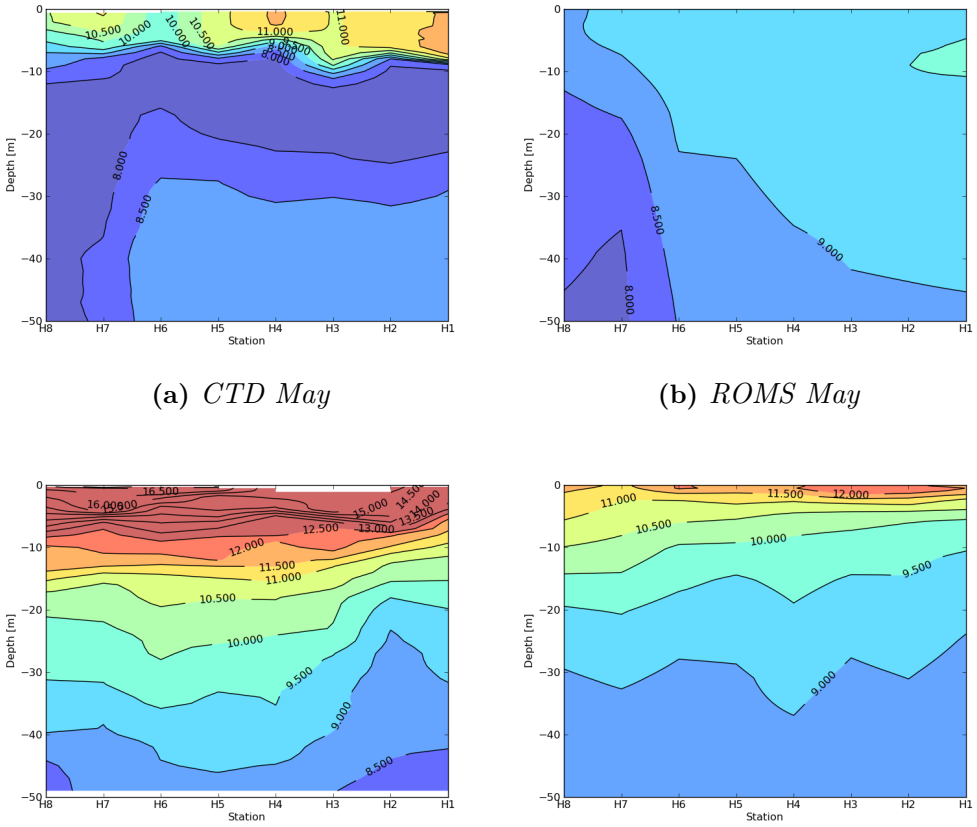

(a) *CTD May*

(b) *ROMS May*

(c) *CTD June*

(d) *ROMS June*

Figure 4.1: *Simulated and measured temperatures [°C] along the Hardangerfjord, 2007*

Salinity

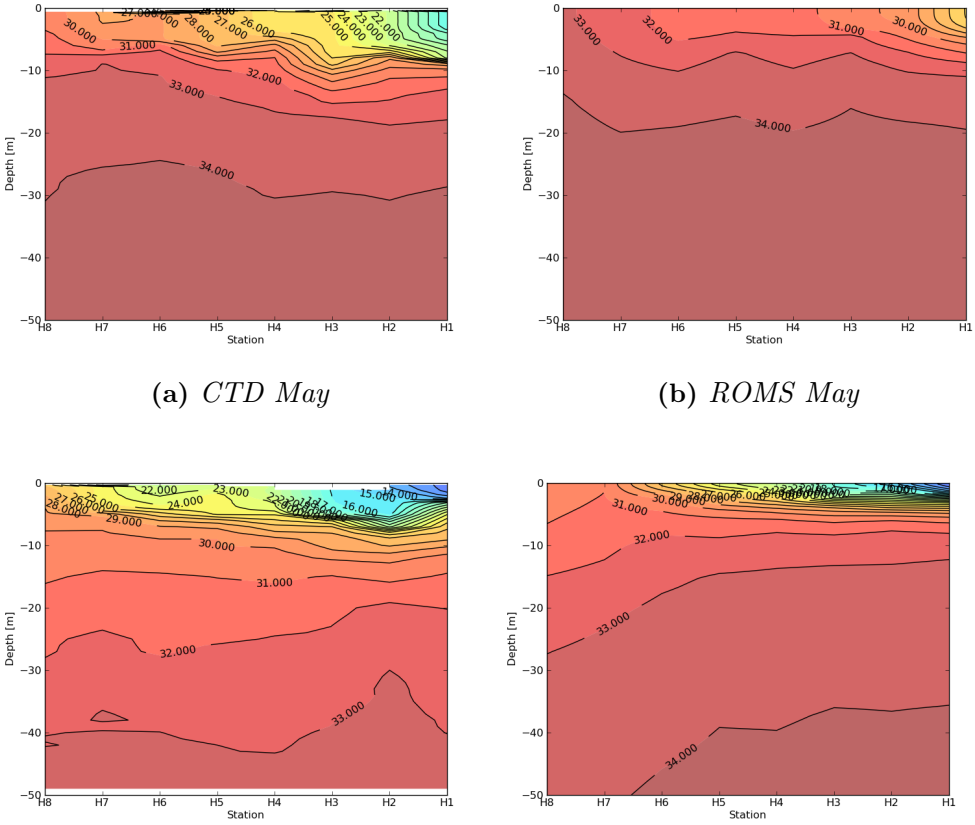

(a) *CTD May* **(b)** *ROMS May*

(c) *CTD June* **(d)** *ROMS June*

Figure 4.2: *Simulated and measured salinity along the Hardangerfjord, 2007*

The observations show typical conditions for the upper 50 m of the fjord with a relatively strong stratification and a warm brackish layer on top. This is a result of heating from the atmosphere, freshwater supply and exchange of coastal water deeper down. In May the temperature is relatively high in the top 5-10 m. At 10-20 m depths the water is colder with a temperature slightly less than 8°C. Under this layer the temperature increases approximately a degree. In July the temperature of the brackish layer is much higher, reaching almost 17°C. The model results do not capture the vertical temperature

gradient well in May, being colder than observations, by 1-2°C in the upper 10 m. Deeper down the differences are less. In July the model simulates the temperature structure better, but with a shallower upper layer still colder than the observed temperatures by 3-4°C. As to salinity, the model do a fairly good job, although it underestimates the brackish surface layer, both the horizontal and vertical extension. The salinity values of the brackish layer is also several units too high in the fjord model results compared to the observations.

The initial condition of the fjord model simulation, as of 15th of April when the simulation started, was taken from the results of the 800 m resolution coastal ocean model. Thus, the initial fields represents a spatially smoothed field and contain possibly less stratification and heat in the surface layer. The forcing of the fjord model is supposed to adjust the results towards a natural situation during a reasonable spin-up time, but still after 22 days obviously this has not yet happened. A month later, in June, the situation is better, and this suggests that it is reasonable to believe that the model results can be improved given a longer spin-up time. The too shallow pycnocline indicates that the model underestimates vertical mixing of the fjord. Reduced vertical mixing might also stem from the spatially smooth wind fields used to force the fjord model, unable to e.g. reproduce the channelling of the wind and the influence of local topography.

Importanct for the salmon lice is the temperature dependent growth. The salmon lice growth is most sensitive to temperature variation for values less then 7°C (Figure 2.3), thus the 1-4°C difference between fjord model results and the observations is less important since the water temperatures mostly are higher than 10°C for the simulated period. As to salinity, the values in the fjord are mostly higher than what the salmon lice is assumed to avoid.

4.1.2 Current

A good representation of the fjord current is the most important factor in the salmon lice modelling. From the ADP observations at the three locations

there is a 56 days overlap of the model results. Time series of 24 hour low-pass filtered current from the observations and the model are compared at 5 m depth for the locations ADP4 and ADP5, and for 18 m from ADP6 (Figure 4.3). Also the frequencies of the currents are calculated, counting the occurrence of every velocity and normalizing the number. Although not completely in phase, the currents appear to be reproduced well in the fjord model. Both the variations in time as amplitudes and duration of the inflow and outflow episodes, as well as the quantitative difference between the three locations are captured by the fjord model.

The mean errors (bias), given by Equation (A.1) in Appendix A, are calculated and given in Table 4.1. The biases are all negative illustrating that the simulated currents are undersetimated directed out of the fjord compared to the observations. The accuracy of the ADP instrument measuring the current is 0.02 m/s (see Appendix A). Hence the biases are barely larger than the accuracy for ADP4 and ADP5, and is less exact than the instrument at ADP6.

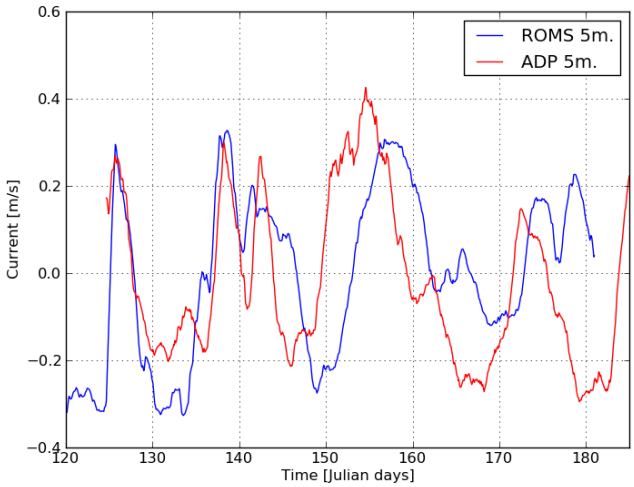

(a) *ADP 4: Current*

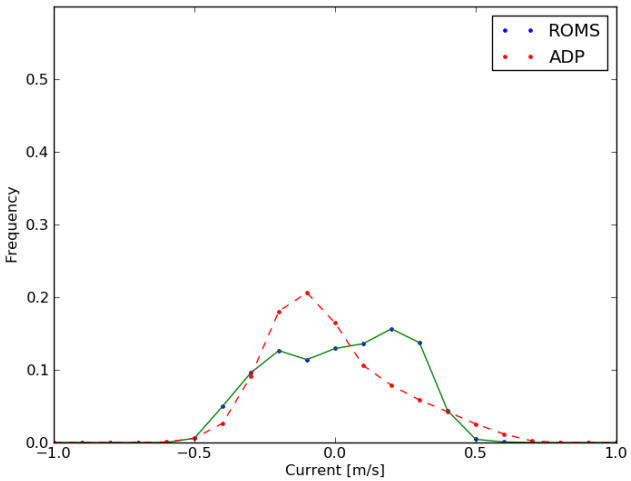

(b) *ADP 4: Frequency*

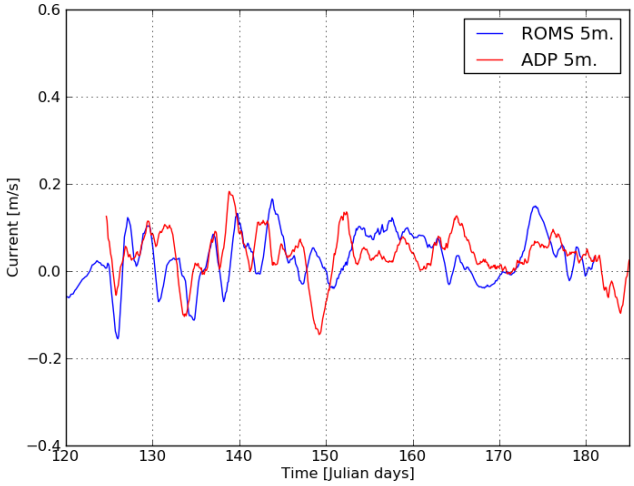

(c) *ADP 5: Current*

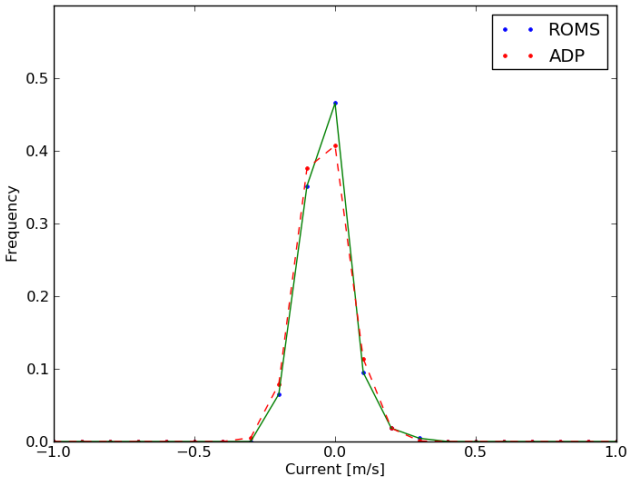

(d) *ADP 5: Frequency*

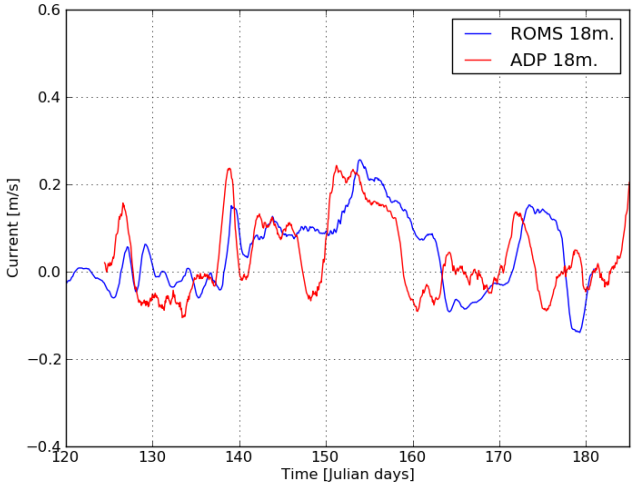

(e) *ADP 6: Current*

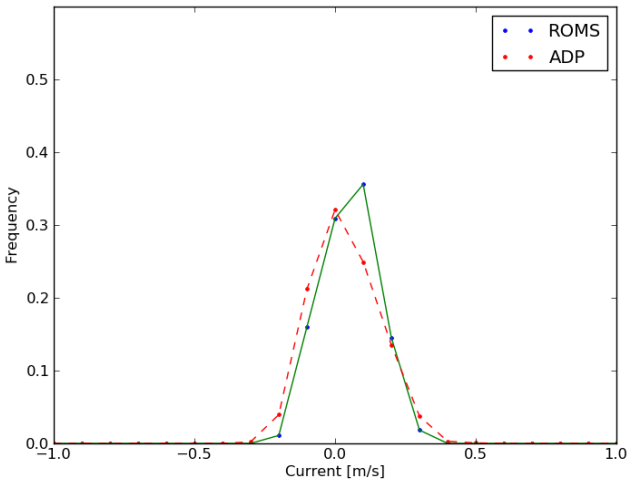

(f) *ADP 6: Frequency*

Figure 4.3: *Time series and frequency of along fjord current. Positive values heading toward the head of the fjord*

Table 4.1: *bias (mean error) for position: ADP4, ADP5 and ADP6*

Station	ADP4	ADP5	ADP6
bias [m/s]	-0.0340	-0.0724	-0.0155

Given that the fjord model calculates an average current for a volume with 200 m $\times$ 200 m horizontal extension, small spatial scale variability occurring in the observations will be filtered out in the model results. Typically the current from numerical model results will underestimate maximum currents in an observational time series. This is also the case here as seen in the frequency plots (Figure 4.3 b, d and f) and especially for ADP4 with the strongest current over all. It is also evident from the frequency plots that the outgoing current (negative values) are underestimated in the fjord model simulation. This must be a result of inadequate forcing, either too little freshwater run-off, wrong winds or wrong boundary condition at the open coastal border.

During deployment and retrieval of the ADPs the instrument drifts along the current. For instance the pressure measurements show that ADP6 was placed at 58 m depth instead of about 30 m as was intended. Since the actual positions of the ADPs are inaccurate and the model has a limited resolution, the agreement of the selected data positions are uncertain.

The model validation clearly shows that the fjord model results include too many discrepancies compared to the observations to accurately represent the conditions of May-June 2007. However, the discrepancies in temperature are not critical for the salmon lice growth, and the currents are shown to be representative for a possible spring period. Thus, the fjord model results will be suitable as a description of a spring situation in the Hardangerfjord and can still be used in the present investigation on salmon lice dispersion.

4.2 Salmon Lice Advection Model

The results from the simulation of salmon lice dispersion given in Chapter 3.3 show us that the dispersion of salmon lice from a single source is highly variable, and support earlier findings [Jones and Beamish, 2011] that lice can move rapidly, potentially long and with large variations. Some of the simulated lice travel more than 100 km from its origin. For all release positions except the innermost (U12), lice were transported out of the Hardangerfjord, along the coastline and into the Bjørnafjord (Figure 1.1). The Norwegian Coastal Current (NCC), placed outside the Hardangerfjord, has typically velocities of 0.2 - 0.5 m/s [Sætre, 2007] giving the lice an efficient transport northwards.

Wind driven currents and internal waves are shown to effectively transport simulated lice with origin close to the mouth fast into the fjord in just a few days days (Figure 3.12 and Figure 3.13). The wind at the coast is the driving force for internal waves as it creates up- and down-welling outside the fjord with horizontal pressure gradients and subsequently long period internal waves creating flow in the upper layer of the fjord. Internal waves are earlier shown to enter the Hardangerfjord regularly [Sundfjord, 2010].

Even if capable to travel long distances, most simulated lice stay within 30 - 50 km from their origin. They seem to accumulate in the small areas creating hotspots. It it assumed that salmon, farmed or from the wild stock, and sea trout bear an enlarged risk of salmon lice infections in these areas. The salmon lice are infective first after 50 dergee-days. Hence, the position they are released at is seldom included in the areas of highest infection pressure.

The simulation of salmon lice has also shown us that modelled lice released only 2.5 km apart can travel to different areas. The large difference seen in dispersion from position U8 and U9 (Figure 3.14) indicates a different circulation pattern on each side of the fjord, presumably due to the Coriolis force. The positions U10 and U11 (Figure 3.14) do not show the same difference in the dispersion, even if the fjord is wider here and the positions

are further apart than for U8 and U9. The explanation is probably that in this part of the fjord, with the open waters north of the island Varaldsøy, more recirculation exists and the model lice released here (U10 and U11) will regularly be transported back and forth between the two positions.

The innermost position (U12) together with the release position placed in the Skåneviksfjord (U6), stands out as positions having the least dispersion of simulated lice (Figure 3.14l and 3.14f). On the other hand this gives the largest abundance of lice in the affected areas. An illustration of the abundance of infectious copepodids in the influence areas of lice from each release position is shown in Figure 4.4. This number will be inversely proportional to the infectious area itself. Obviously the average density increases into the narrower parts of the fjords, i.e. also the areas of the lower current speeds.

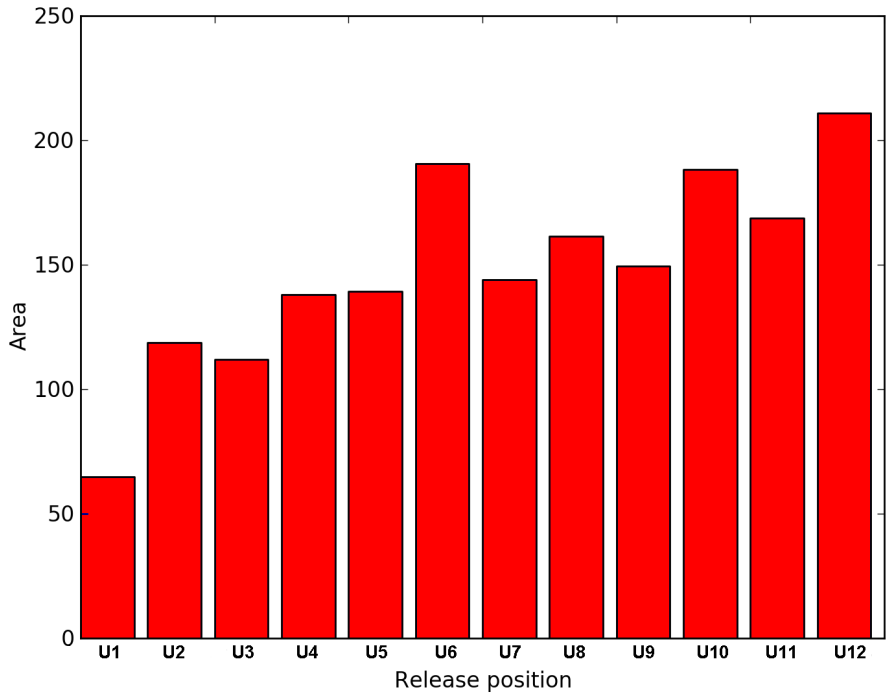

Figure 4.4: *Area* (km^2) *affected with density* 10^{-3} *Copepodites per* m^3 *or more of simulated salmon lice, 2007.*

The calculated influence areas of salmon lice from the different release positions (Figure 3.14) are all large, but the density of copepodids vary a lot within these areas. It is likely that the density needs to be of a certain level before representing an efficient infection pressure on salmon and sea trout. This critical level of copepodits density is unknown, but this concept of infectious dose needs to be elaborated further in the future. The fish farms location, and their levels of lice is known. Contemporary the IMR has performed measurements of salmon lice on wild fish at different locations in the fjord for over a decade, building up an understanding of salmon lice abundance variability in time and space [Bjørn et al., 2011]. The salmon lice model can support this effort by simulating realistic amounts of lice, released at genuine positions in the fjord, and compare the simulated dispersion to

IMRs measurements of lice on fish. By comparison it might be possible to establish a threshold of copepodid density or necessary dose for infection of salmon lice on salmonid fish. Once this dose is found, the influence area of salmon lice from different release positions in the fjord can be more precisely found using numerical models.

The large infectious areas of salmon lice from all the different release positions indicate that areas of fallowing in the fjord will not be able to block possible infection from other areas nearby unless the necessary dose for infection is high. The higher this critical density of salmon lice is found to be, the less the areas fallowed need to cover in order to work as a blockage. The fallow regions will certainly reduce the density of lice in an area, probably notably for both farmed and wild salmon, but they might not be more efficient than an evenly distributed decrease of biomass in the area. For instance release positions U4 and U5 have close to identical dispersion of salmon lice and hence infectious areas and copepodid concentrations (Figure 3.14d and 3.14e) and it is clear that fallowing an area including only one of these positions would decrease the total amount of lice in the affected area, but not creating a zone free from lice.

As the farmed fish is trapped at a location, making it possible to delouse from time to time, the wild stock of salmon and sea trout seems to be the most sensitive to lice infestations [Bjørn et al., 2011]. The vulnerable post-smolt have to migrate out of the fjord without gaining a mortal amount of salmon lice in order to keep the wild stock at a sustainable level. As the dispersion of salmon lice mainly is directed into the fjord from the outer release positions (Figure 3.14), fallow regions should be placed between the coast and the river the post-smolt originates from. A strategy to reduce the salmon lice load for the locally residing sea trout seems more difficult using small fallowed areas.

The dispersion of simulated lice from the outer part towards the head of the fjord due to currents driven by wind and internal waves may indicate that a delousing event starting at the coast and sequencing inwards would be

favourable. As the salmon lice are infectious for approximately 100 degree-days (10 days at temperature of 10°C), a fish farm might have been a source of infections after being deloused. They are even in danger of infecting themself after a delousing event.

CHAPTER 5

Conclusion

The simulated currents used in the thesis are shown to be representative of the Hardangerfjord. The inadequate forcing make the direct comparison with the conditions in 2007 less relevant.

In addition to reveal the typical current patterns of the upper ∼100 m of the water column in the fjord, like the brackish layer flow, the wind driven flow and the tide, including the water mass distributions, the results show how an internal wave generated by coastal down-welling outside the Hardangerfjord is propagating all the way into the main fjord during 6 days. The associated upper layer water exchange with this wave is potentially large estimated to ∼50% of the volume in the upper 15 m of inner parts of the fjord for a single event. A closer examination of this exchange process is outside the scope of this thesis, other than such events are important transport mechanisms for salmon lice.

The hypothesises raised in the introduction were:

1. Lice do disperse differently depending on which part of the fjord they originate from.

2. It is possible to define an area that is influenced by lice originating from a given position.

3. The influence area of lice from a given position can be used to estimate the size of the regions of synchronized delousing and fallowing.

Both the two first hypothesises cannot be falsified, since it indeed is shown differences in salmon lice distribution given their origin and that lice from certain origins can mainly end up within a definite area. Although infectious salmon lice copepodids potentially reside all over the fjord, with the influence areas of lice from the different release positions ranging from 1300 km^2 to over 4000 km^2, the spatial variations of copepodid densities are large with substantially higher values in hot spots like bays, narrows and along shorelines. Thus, unless only a tiny concentration is needed to infect salmon fish, there are different distribution patterns in the fjord that are dependent of the lice origin. However, finding the extensions of these areas are depending on more knowledge on critical doses of salmon lice needed to infect salmonid fish, if such exists.

The third hypothesis is harder to evaluate. As the knowledge of the relation between abundance and infections of salmon lice on salmonid fish is limited, areas of delousing and fallowing are not easily defined. A higher critical dose of salmon lice will result in a smaller area needed to fallow in order to work as a blockage. The practise of fallowing is however not pointless as they reduce the total biomass in certain periods and hence the potential amount of lice in the area. The large transport of salmon lice into the fjord in periods as simulated by the model due to wind driven currents and internal waves, indicates that a synchronized delousing process starting in the outer part and continuing inwards would be favourable. Fallow areas in order to reduce salmon lice as threat for the post-smolt migrating from rivers in the fjord and to the sea should if possible cover the migration route. A strategy to reduce the salmon lice load for the sea trout that are resident in the fjord, seems more difficult.

CHAPTER 6

Future work

Since the history of salmon lice modelling is only 10 years old, improvements of this method is necessary and expected. In this thesis the simulation of salmon lice dispersion is only done for the spring 2007, as this was the only period with available current model results. Obviously the inter annual variation of water temperature in the fjord will affect the development time of salmon lice. Especially at lower temperatures (under 7°C) the duration of the infectious copepodid stage is assumed to be sensitive to temperature variations. The dispersion of salmon lice can be assumed to increase with decreasing temperatures. Hence, simulations of salmon lice at all seasons and for different years will be of interest.

Numerical simulations always need continuously validation and they may have room for improvements. The fjord current model should be given a longer spin-up period than what was available in this thesis, as well as better resolution of the atmospheric forcing. The coastal current model used for boundary conditions at the open boundary of the fjord model should as well be continuously monitored and validated. It should be mentioned that the

practise today at IMR would have provided fjord model results in agreement with these recommendations.

Both swimming and no swimming particles have been found to be trapped at the pycnocline and along fronts, beyond what can be explained by physiological response of the organisms [Franks, 1992]. This accumulation has been found both using mathematical models [Franks, 1992] and for zooplankton in nature [Hunt Jr, 1997]. Examination of to what extent this applies for the salmon lice, and should be included in numerical models is clearly of interest.

Given fjord model results validated to represent certain periods of time, realistic emissions at its genuine position should be performed. The salmon lice model should produce a relative abundance of lice from the different sources, and these results should be compared to observations of salmon lice in the fjord and possibly be able to quantify at which copepodid densities the salmonid fish are in risk of infections.

Coupling the simulations of salmon lice with fish migration models of salmon and sea trout, we might be able to quantify the influence of salmon lice on the wild stock. Hence one can establish a maximum biomass and the distribution of farmed fish in a fjord that the wild stock is able to sustain at a viable level.

Today the fish farms are placed at positions exposed to currents of a certain magnitude in order to maintain water exchange at a certain cage level to supply oxygen and remove waste. At the same time too strong currents should be avoided, as it deforms the closing net and decrease the area inside [Oppedal et al., 2011]. The location of the fish farms are not chosen from knowledge of salmon lice abundance, however such information should in the future be included when considering biomass and suitable fish farm positions in a fjord.

Bibliography

J. Albretsen, A.K. Sperrevik, A. Staalstrøm, A.D. Sandvik, F. Vikebø, and L. Asplin. Norkyst-800 report no.1 user manual and technical descriptions. *Fisken og havet*, 2, 2011.

L. Asplin, A.G.V. Salvanes, and J.B. Kristoffersen. Nonlocal wind-driven fjord-coast advection and its potential effect on plankton and fish recruitment. *Fisheries Oceanography*, 8:4, 1999.

J. Aure, 2011. Personal comunication.

J.J. Bengtsen. Vertikal fordeling af lakselusens (lepeophtheirus salmonis) planktoniske stadier: Effekten af salinitet, lys og morke. 2011. Joint Nordic Master's Programme in Marine Ecosystems and Climate, Universities of Bergen, Iceland, Aarhus and the Faroe Islands.

P.A. Bjørn, B. Finstad, L. Asplin, O. Skilbrei, R. Nilsen, R.M.S. Llinares, and K.K. Boxaspen. Metodeutvikling for overvåkning og telling av lakselus på viltlevende laksefisk. *Rapport fra havforskningen*, 8, 2011.

K. Boxaspen and T. Næss. Development of eggs and the planktonic stages of

salmon lice (lepeophtheirus salmonis) at low temperatures. *Contributions to Zoology*, 69(1/2):51–56, 2000.

B. Cushman-Roisin, L. Asplin, and H. Svendsen. Upwelling in broad fjords. *Continental Shelf Research*, 14(15):1701 – 1721, 1994. ISSN 0278-4343. doi: 10.1016/0278-4343(94)90044-2. URL `http://www.sciencedirect.com/science/article/pii/0278434394900442`.

J. G. Davidsen, N. Plantalech Manel-la, F. Økland, O. H. Diserud, E. B. Thorstad, B. Finstad, R. Sivertsgård, R. S. McKinley, and A. H. Rikardsen. Changes in swimming depths of atlantic salmon *Salmo salar* post-smolts relative to light intensity. *Journal of Fish Biology*, (73):1065–1074, 2008.

D.P. Dee. *Quantitative Skill Assessment for Coastal Ocean Models*. Americal Geophysical Union, Washington DC., 1995.

Directory of Fisheries, 2011. URL `http://fiskeridir.no`. Downloaded 01.10.2011.

B. Ådlandsvik and S. Sundby. Modelling the transport of cod larvae from the lofoten area. *ICES Journal of Marine Science Symposium*, 198, 1994.

A. Ervik, A.L. Agnalt, L. Asplin, J. Aure, T.C. Bekkvik, I. Døskeland, A. A. Hageberg, T. Hansen, Ø Karlsen, F. Oppedal, and Ø Strand. Akvavis - dynamisk gis-verktøy for lokalisering av oppdrettsanlegg for nye oppdrettsarter. *Fisken og havet*, 10, 2008.

D. M. Farmer and H. J. Freeland. The physical oceanography of fjords. *Prog. Oceanogr.*, 12, 1983.

Peter J. S. Franks. Sink or swim: accumulation of biomass at fronts. *Mar. Ecol. Prog. Ser.*, 82, 1992.

H.G. Gade. Features of fjord and ocean interaction. *The Nordic Seas: Berlin, Springer*, pages 182–189, 1986.

A.E. Gill. *Atmosphere-ocean dynamics*. Academy Press, 1982.

S. Gudjonsson, I.R. Jonsson, and T. Antonsson. Migration of atlantic salmon, salmo salar, smolt through the estuary area of river ellidaar in iceland. *Environmental Biology of Fishes*, 74(3):291–296, 2005.

P.A. Heuch. Experimental evidence for aggregation of salmon louse copepodids (lepeophtheirus salmonis) in step salinity gradients. *Journal of the Marine Biological Association of the UK*, 75:927–939, 1995.

P.A. Heuch and H.E. Karlsen. Detection of infrasonic water oscillations by copepodids of lepeophtheirus salmonis (copepoda caligida). *Journal of Plankton Research*, 19(6):735, 1997.

P.A. Heuch and T.A. Mo. A model of salmon louse production in norway: effects of increasing salmon production and public management measures. *Diseases of aquatic organisms*, 45(2):145–152, 2001.

P.A. Heuch, A. Parsons, and K. Boxaspen. Diel vertical migration: A possible host-finding mechanism in salmon louse (lepeophtheirus salmonis) copepodids? *Can. J. Fish. Aquat. Sci*, 52:681–689, 1995.

J.R. Hunt Jr. Physics, zooplankton, and the distribution of least auklets in the Bering Sea - a review. *ICES Journal of Marine Science*, 54, 1997.

S.C. Johnson and L.J. Albright. The developmental stages of lepeophtheirus salmonis ((krøyer, 1837)(copepoda: Caligoida). *Canadian Journal of Zoology*, 69:929–950, 1991a.

S.C. Johnson and L.J. Albright. Development, growth, and survival of lepeophtheirus salmonis (copepoda: Caligidae) under laboratory conditions. *Journal of the Marine Biological Association of the UK*, 71(02):425–436, 1991b.

S. Jones and R Beamish. *Salmon Lice: An Integrated Approach to Understanding Paracite Abundance and Distribution*. WILEY - BLACKWELL, 1st edition, 2011.

myroms.org. Dokumentation portal, 2011. URL `http://www.myroms.org/`. Downloaded: 01.06.2011.

Nortek AS. Aquadopp profiler, 2006. URL `http://www.nortek_as.com`. Downloaded 07.09.2010.

F. Oppedal, Gansel L. Stien, J.H., P. Klebert, P. Lader, J. Guenther, M. Remen, T.S. Aas, J. Aure, and T. Torgersen. Havforskningsrapporten, 2011.

H. Otterå, O. Skilbrei, Ø. Skaala, K. Boxaspen, J. Aure, G.L. Taranger, A Ervik, and R Borgstrøm. The hardanger fjord - salmonid aquaculture and effects on wild salmonid populations. 2004.

L.E. Petterson. Beregning av totalavløp til hardangerfjorden. 2008. Norges vassdrags- og energidirektorat.

S Pond and G.L. Pickard. *Introductory Dynamical Oceanography*. 1983.

A.D. Sandvik, 2010-2011. Personal comunication.

A. Stien, P.A. Bjørn, P.A. Heuch, and D.A. Elston. Population dynamics of salmon lice lepeophtheirus salmonis on atlantic salmon and sea trout. *Marine Ecology Progress Series*, 290:263–275, 2005.

A Stigebrandt. Some aspects of tidal interaction with fjord constrictions. *Estuarine and Coastal Marine Science*, 2, 1980.

R Sætre. *The Norwegian Coastal Current -Oceanography and Climate*. Institute of Marine Research, 1st edition, 2007.

R. Sætre, J. Aure, and R. Ljøen. Wind effects on the lateral extension of the norwegian coastal water. *Continental Shelf Research*, 8(3):239–253, 1988.

V.N. Sundfjord. Volume transport due to coastal wind-driven internal pulses in the hardangerfjord. 2010. UiO.

H. Svendsen and R.O.R.Y. Thomsom. Wind-driven circulation in a fjord. *Journal of Physical Oceanography*, 8, 1978.

H. Svendsen, N. Utne, and H. Thomsen. Hydrografi i hardangerfjorden (feb.-sept. 1972). *Rådgivende utvalg for fjordundersøkelser : Hardangerfjord-prosjektet. Preliminær rapport*, 1972-73.

E. Thorstad, F. Økland, B. Finstad, R. Sivertsgård, P. Bjørn, and R. McKinleyd. Migration speeds and orientation of atlantic salmon and sea trout post-smolts in a norwegian fjord system. *Environmental Biology of Fishes*, 71(3):305–311, 2004.

J.M. Wallace and P.V. Hobbs. *Atmospheric Science: An Introductory Survey.* 2nd edition, 2006.

APPENDIX A

Appendix

A.1 The Equation of Mean Error (bias)

$$bias = \frac{\sum_{i=1}^{N}(X_i - Y_i)}{N} \tag{A.1}$$

N = number of measurements X = Measurement Y = Model

A.2 The setup and accuracy of the Nortek Aquadopp Profiler

Table A.1: *Nortek Aquadopp Profiler set-up and accuracy, used spring 2007*

Nr cells	40
Cell size	1 m
Horizontal accuracy	0.021 m/s
Vertical Accuracy	0.007 m/s
Blanking distance	1 m
Sampling intervall	3600 sek